To appear in *the Astrophysical Journal*
Preprint typeset using LaTeX style emulateapj

GRADIENTS OF ABSORPTION LINE STRENGTHS IN ELLIPTICAL GALAXIES

Chiaki KOBAYASHI
Department of Astronomy, School of Science, University of Tokyo
7-3-1, Hongo, Bunkyo-ku, Tokyo 113-0033, Japan;
e-mail: chiaki@astron.s.u-tokyo.ac.jp
Nobuo ARIMOTO
Institute of Astronomy, School of Science, University of Tokyo
2-21-1, Osawa, Mitaka, Tokyo 181-8588, Japan;
e-mail: arimoto@mtk.ioa.s.u-tokyo.ac.jp

ABSTRACT

We have re-studied line-strength gradients of 80 elliptical galaxies. Typical metallicity gradients of elliptical galaxies are $\Delta[\mathrm{Fe/H}]/\Delta\log r \simeq -0.3$ which is flatter than the gradients predicted by monolithic collapse simulations. The metallicity gradients do not correlate with any physical properties of galaxies, including central and mean metallicities, central velocity dispersions σ_0, absolute B-magnitudes M_B, absolute effective radii R_e, and dynamical masses of galaxies. By using the metallicity gradients, we have calculated mean stellar metallicities for individual ellipticals. Typical mean stellar metallicities are $\langle[\mathrm{Fe/H}]\rangle \simeq -0.3$, and range from $\langle[\mathrm{Fe/H}]\rangle \simeq -0.8$ to $+0.3$, which is contrary to what Gonzalez & Gorgas (1996) claimed; the mean metallicities of ellipticals are not universal. The mean metallicities correlate well with σ_0 and dynamical masses, though relations for M_B and $\mathrm{R_e}$ include significant scatters. We find fundamental planes defined by surface brightnesses $\mathrm{SB_e}$, $\langle[\mathrm{Fe/H}]\rangle$, and R_e (or M_B), and the scatters of which are much smaller than those of the $\langle[\mathrm{Fe/H}]\rangle$ - R_e (or M_B) relations. The $\langle[\mathrm{Fe/H}]\rangle$ - $\log\sigma_0$ relation is nearly in parallel to the $[\mathrm{Fe/H}]_0$ - $\log\sigma_0$ relation but systematically lower by 0.3 dex; thus the mean metallicities are about a half of the central values. The metallicity-mass relation, or equivalently, the color-magnitude relation of ellipticals holds not only for the central part but also for the whole part of galaxies. Assuming that $\mathrm{Mg_2}$ and $\mathrm{Fe_1}$ give [Mg/H] and [Fe/H], respectively, we find $\langle[\mathrm{Mg/Fe}]\rangle \simeq +0.2$ in most of elliptical galaxies. $\langle[\mathrm{Mg/Fe}]\rangle$ shows no correlation with galaxy mass tracers such as σ_0, in contrast to what was claimed for the central [Mg/Fe]. This can be most naturally explained if the star formation had stopped in elliptical galaxies before the bulk of Type Ia supernovae began to explode. Elliptical galaxies can have significantly different metallicity gradients and $\langle[\mathrm{Fe/H}]\rangle$ even if they have the same galaxy mass. This may result from galaxy mergers, but no evidence is found from presently available data to support the same origin for metallicity gradients, the scatters around metallicity-mass relation, and dynamical disturbances. This may suggest that the scatters have their origin at the formation epoch of galaxies.

Subject headings: galaxies: abundances — galaxies: elliptical — galaxies: evolution — galaxies: formation

1. INTRODUCTION

How elliptical galaxies formed is one of key questions of modern astronomy. Two competing scenarios have so far been proposed: Elliptical galaxies should form monolithically by gravitational collapse of gas cloud with considerable energy dissipation (e.g., Larson 1974b; Arimoto & Yoshii 1987), or alternatively ellipticals should form via mergers of relatively small galaxies (e.g., Toomre & Toomre 1972; Kauffmann & White 1993; Cole et al. 1994). Elliptical galaxies show apparently little evidence for ongoing star formation, the bulk of their stars are old (e.g., Kodama & Arimoto 1997; Stanford, Eisenhardt, & Dickinson 1997; Kodama et al. 1998a), and yet some of ellipticals show strong signs of recent dynamical disturbances (Schweizer et al. 1990; Schweizer & Seitzer 1992). Observational evidences are confusing and controversial.

The merger hypothesis assumes that gaseous disk-like galaxies formed first by assembling subgalactic clumps, then two grown-up disk galaxies of similar mass collided into a single giant elliptical galaxy (e.g., Kauffmann & White 1993; Kauffman & Charlot 1998). Alternatively, an elliptical galaxy could form if many small galaxies accreted onto a massive disk galaxy (e.g., Cole et al. 1994; Baugh et al. 1998). Observationally, the dynamical disturbances such as shells/ripples, transient dust lanes, and multiple and/or counter-rotating cores (e.g., Kormendy & Djorgovski 1989) all seem to support the scenario that elliptical galaxies formed via hierarchical clustering of smaller galaxies (Schweizer & Seitzer 1992), which is a picture predicted by cold dark matter (CDM) cosmology. The merger hypothesis may easily explain morphology-density relation of galaxies in clusters (Dressler 1980; Dressler et al. 1997), a significant number of interacting galaxies at high redshifts (Driver, Windhorst, & Griffiths 1995), Butcher-Oemler effects (Butcher & Oemler 1978; 1984), and E+A galaxies (Dressler & Gunn 1983; 1992). However, collisions and mergers of galaxies should be less frequent at the cluster center because of large velocity dispersions of galaxies there (Ostriker 1980). A recent HST observation reveals conspicuous spiral arms dominated by A-type stars in the E+A galaxies (Franx et al. 1996), which suggests that the Butcher-Oemler galaxies are not ellipticals, but spiral galaxies falling onto a cluster potential for the first time

and are witnessed at an instance of being transformed into S0 galaxies. Elliptical galaxies are surrounded by a huge number of globular clusters (GCs). The number of globular clusters per galaxy luminosity (specific frequency) is almost twice of that in spiral galaxies (Harris 1991). If ellipticals formed via mergers of spiral galaxies, at least similar amount of GCs should be born during the merger events (van den Bergh 1982; 1990). True, young GCs are discovered in merging galaxies (Whitmore & Schweizer 1995), but these GCs are far less numerous than those required for explaining high specific frequencies of ellipticals. On the other hand, GCs in elliptical galaxies have bimodal [Fe/H] distributions (Forbes, Brodie, & Grillmair 1997), which has been considered to support the merging hypothesis.

The dissipative collapse hypothesis assumes that a bulk of stars in ellipticals formed during an initial burst of star formation, which was induced by the collisions of fragmented clouds in proto-galaxies, and terminated by a supernovae-driven galactic wind that expelled the left-over interstellar gas from galaxies (e.g., Larson 1974b; Arimoto & Yoshii 1987). The galactic wind is supposed to play an essential role in enriching heavy elements in hot intracluster gas (Ciotti et al. 1991). Elliptical galaxies after the wind should evolve passively (Kodama et al. 1998a). The shells and ripples would appear when ellipticals captured nearby dwarf galaxies. These dynamical disturbances would be detectable for a couple of Gyrs, but the capture itself would not introduce any significant change in the stellar constituents of galaxies, since the mass involved in the secondary formation of stars is at most 10% as the study of Hβ absorption and broad band colors of elliptical galaxies shows (Kodama & Arimoto 1998). The galactic wind predicts tight correlations among global properties of galaxies including a color-magnitude relation (Bower, Lucey, & Ellis 1992) and a fundamental plane (Djorgovski & Davies 1987; Dressler et al. 1987). Recent observations of clusters at high redshifts confirm that these relationships are holding even at $z \sim 1$ (Dickinson 1996; Schade, Barrientos & Lopez-Cruz 1997; Kelson et al. 1997; Stanford et al. 1998). A progressive change of the color-magnitude relation as a function of look-back time clearly indicates that a bulk of stars in ellipticals formed at the redshift $z_{\rm f} \gtrsim 2.5 - 4$ (Kodama et al. 1998a).

In this paper, we study gradients of absorption line strengths of elliptical galaxies. In the last two decades, the line strength gradients of ellipticals were extensively studied by Faber (1977; F77), Efstathiou & Gorgas (1985; EG), Couture & Hardy (1988; CH), Peletier (1989, PEL), Gorgas, Efstathiou, & Aragón-Salamanca (1990; GEA), Boroson & Thompson (1991; BT), Davidge (1991a; D91a), Davidge (1991b; D91b), Bender & Surma (1992; BS), Davidge (1992, D92), Carollo, Danziger, & Buson (1993; CDB), Davies, Sadler, & Peletier (1993; DSP), Gonzalez (1993; GON), Hes & Peletier (1993; HP), Saglia et al. (1993; SAG), Carollo & Danziger (1994a; CDa), Carollo & Danziger (1994b; CDb), Sansom, Peace, & Dodd (1994; SPD), Cardiel, Gorgas, & Aragón-Salamanca (1995; CGA), and Fisher, Franx, & Illingworth (1995b; FFI). Major lines so far studied are $\rm Mg_2$, $\rm Mg_b$, $\rm Fe_1(5270\AA)$, $\rm Fe_2(5335\AA)$, Hβ, and Hγ lines. The first four metallic lines are degenerate in age and metallicity, while the two hydrogen lines are sensitive to stellar age (Burstein et al. 1984; Faber et al. 1985; Gonzalez 1993; Worthey 1994). Recently, Vazdekis & Arimoto (1999) have broken up the age-metallicity degeneracy of Hγ by including neighboring metallic lines in such a way that a resulting Hγ depends only on age. The approach is thus very promising, but no attempt has yet been conducted for estimating ages of giant ellipticals. We therefore should keep it in our mind that some of giant elliptical galaxies in the field might be significantly younger than cluster ellipticals (Franceschini et al. 1998; Kodama, Bower, & Bell 1998b) and that the radial gradients of metallic lines may be caused by not only a radial variation of stellar metallicity but also an equivalent variation of mean stellar age. This paper discusses the gradients of the four metallic lines and Hβ, but mainly $\rm Mg_2$ and $\rm Mg_b$ gradients, because $\rm Fe_1$ and $\rm Fe_2$ are easily influenced by a possible gradient of stellar velocity dispersion whose spatial distribution in a galaxy is still difficult to measure precisely.

Previous studies showed that $(\rm Mg_2)_0$ correlate with the velocity dispersion σ_0 at the galaxy center (Davies et al. 1987; Burstein et al. 1988; Bender, Burstein, & Faber 1993). A similar relation holds for $(\rm Mg_2)_0$ and total absolute magnitudes M_B (Faber 1973; Burstein 1979; Terlevich et al. 1981; Dressler 1984). If, *admittedly a big if*, one can assume that elliptical galaxies are old, one can convert $\rm Mg_2$ into the metallicity Z either empirically (Burstein et al. 1984; Faber et al. 1985) or theoretically with a help of population synthesis models (Mould 1978; Peletier 1989; Buzzoni, Gariboldi, & Mantegazza 1992; Barbuy 1994; Worthey 1994; Casuso et al. 1996; Bressan, Chiosi, & Tantalo 1996; Kodama & Arimoto 1997). For example, if Worthey's (1994) calibration is adopted, one finds that a *typical* metallicity gradient of elliptical galaxies is $\Delta \log Z / \Delta \log r \simeq -0.3$. The radial gradient of metallic line strength can be naturally explained by the dissipative collapse picture. However, the measured gradients are less steep than those predicted by numerical simulations of collapse model: For example, Larson's hydrodynamical simulations gave $\Delta \log Z / \Delta \log r \sim -0.35$ (Larson 1974a), and -1.0 (Larson 1975); Carlberg's N-body simulations gave $\Delta \log Z / \Delta \log r \sim -0.5$ (Carlberg 1984). This discrepancy could be interpreted if mergers make an original gradient flattened; indeed numerical simulations showed that the gradient in a disk galaxy should be halved after three successive mergers of galaxies with similar size (White 1980). However, both simulations of the dissipative collapse and successive mergers leave room for the improvements, because some essential physical processes such as star formation, thermal feedback from supernovae, and metal enrichment were not taken into account.

Elliptical galaxies with larger values of $(\rm Mg_2)_0$ tend to show steeper $\rm Mg_2$ gradients (Gorgas et al. 1990; Carollo et al. 1993; Gonzalez & Gorgas 1996). Since a brighter elliptical usually has a larger $(\rm Mg_2)_0$ (Davies & Sadler 1987), Gorgas & Gonzalez (1996) suggested that a larger $(\rm Mg_2)_0$ is cancelled by a steeper gradient and that elliptical galaxies should have very similar mean stellar metallicities, regardless of their luminosities and masses. If this is true, the color-magnitude relation is nothing but a *local* relation that holds only for the central part of a galaxy and may not reflect the formation process of ellipticals. One should

use global metallicities instead of local ones in studying the origin of ellipticals. Therefore, it is particularly important to estimate accurately mean stellar metallicities of ellipticals and study relations with other global features of galaxies.

No tight correlations between the Mg_2 gradient and other properties of galaxies are yet confirmed. The Mg_2 gradient and the central velocity dispersion σ_0 may correlate (Davidge 1992) but with a significant scatter (Gorgas et al. 1990), and cD galaxies deviate from that relation considerably (Carollo et al. 1993). However, Davies et al. (1993) did not find any significant correlation between the Mg_2 gradient and σ_0. Nevertheless, the local colors and the line-strengths correlate tightly (Davies et al. 1993; Carollo & Danziger 1994a) and both show strong correlation to the local escape velocity (Franx & Illingworth 1990; Davies et al. 1993; Carollo & Danziger 1994a). Elliptical galaxies which deviate considerably from the ridge line of Mg_2 – absolute magnitude relation tend to have larger values of Σ, a degree of dynamical disturbances (Schweizer et al. 1990), but the Mg_2 gradient is not correlated to Σ, nor the isophotal shape a_4/a (Davidge 1992).

If elliptical galaxies formed monolithically from a massive gas cloud, the Mg_2 gradient should correlate with global properties of galaxies. Carlberg (1984) showed that more massive galaxies have steeper metallicity gradients. Apparent lack of such correlations may suggest that the Mg_2 gradient was built up via a series of successive mergers of gas-rich galaxies. The situation surrounding Mg_2 gradient studies is complicated and confusing. This we believe is due to a lack of suitable sample of the Mg_2 gradient. A total exposure time required to measure the Mg_2 gradient is much longer than that for broad band color gradients. Therefore, a single group of authors can observe only a limited number of galaxies. What is worse, a quality of data is not uniform. We have studied 187 line strength gradients of 133 early-type galaxies. After carefully examining the quality of data, we have chosen data for 80 elliptical galaxies. Section 2 describes how the data are selected and analyzed. Section 3 gives a definition of the mean stellar metallicities of ellipticals. Section 4 gives our main results, and our discussions and conclusions are given in section 5 and section 6, respectively.

2. LINE STRENGTH GRADIENTS

2.1. *Line Strength Gradients*

We have studied 187 gradients of Mg_2, Mg_b, Fe_1 ($5270\AA$), Fe_2 ($5335\AA$), and Hβ for 133 early-type galaxies. Data are taken from 20 data sources; F77, EG, CH, PEL, GEA, BT, D91a, D91b, BS, D92, CDB, DSP, GON, HP, SAG, CDa, CDb, SPD, CGA, and FFI. To demonstrate a global view of line-strength gradients, we summarize Mg_2 and Mg_b gradients of these galaxies in Appendix A. Unfortunately, accurate and precise line-strength gradient data are difficult to obtain, requiring long integrations on bright objects with large telescopes to obtain high-enough S/N ratio (e.g., DSP; GON); thus qualities of these data are not uniform, and we are obliged to abandon many of them due to poor qualities as described below (we are indebted to the anonymous referee for reminding us different qualities of the gradient data, and are helped considerably with the referee's comments in making the following brief descriptions for the data sources, but we are entirely responsible for any critical remarks we made): **F77** – poor data quality, no errorbars in figures, but quite large, the sky subtraction is poor, and perhaps no velocity dispersion correction [trustworthiness = (index strengths, gradients) = (fair, poor)]; **CH** – data quality is poor outside nucleus, the gradients are uncertain, and the sky subtraction is poor [trustworthiness = (poor, poor)]; **PEL** – the calibration is suspicious, and the errorbars may be underestimated [trustworthiness = (good, good)]; **GEA, EG** – data quality is poor outside nucleus, errors are large, the sky subtraction is poor, and the velocity dispersion correction may not be done [trustworthiness = (fair, poor)]; **BT** – the quality of spectra is poor outside nucleus, the sky subtraction is poor, the errorbars are not given, but the velocity dispersion correction is reasonable [trustworthiness = (fair, good)]; **D91a, D91b, D92** – the calibrations are suspicious, data quality is reasonable for two of three galaxies, sky subtraction is poor, but it is not clear if velocity dispersion correction is done or not [trustworthiness = (poor, fair?)]; **BS** – the calibration is good, but the sky subtraction is suspicious, velocity dispersion corrections? [trustworthiness = (fair, fair)]; **CDB** – except for Mg_2, the calibration is uncertain, significant contamination of emissions in galaxy spectra [trustworthiness = (good, excellent)]; **DSP** – the calibration is done carefully, the sky subtraction is suspicious but better than most [trustworthiness = (excellent, excellent)]; **GON** – the calibration is excellent except for Mg_1 and Mg_2 which are affected by chromatic focus variations, for Hβ the velocity dispersion correction is suspicious [trustworthiness = (excellent, excellent)]; **HP** – the calibration is suspicious [trustworthiness = (good, good)]; **SAG** – zero-points of indices are off, and the velocity dispersion correction is suspicious [trustworthiness = (poor, good)]; **CDa, CDb** – the calibrations are uncertain for Fe_1 and Fe_2, and the sky subtraction is suspicious [trustworthiness = (good, excellent)]; **SPD** – uncalibrated, the sky subtraction is poor, and the velocity dispersion correction is probably wrong [trustworthiness = (poor, poor)]; **CGA** – the calibration is off by 0.014 mag, and the velocity dispersion correction is not done [trustworthiness = (poor, poor)]; **FFI** – the calibration is uncertain, the sky subtraction and velocity dispersion correction are good, but the emission contamination is observed with [OIII] [trustworthiness = (good, excellent)].

Among these 20 data sources, we have adopted 5 references (BS, CDB, DSP, CDa, and CDb) that provide excellent Mg_2 gradient data for 46 ellipticals and 2 references (GON and FFI) that give high quality Mg_b gradient data for additional 34 elliptical galaxies. These authors almost universally used CCDs as detectors instead of photon counters, due to unreliability of the wavelength and flux calibrations of photon counters (e.g., Peletier 1989; Trager et al. 1998).

We apply a linear regression analysis for the line-strength gradients by taking account of observational errors:

$$\mathrm{Index}(r) = (\mathrm{Index})_{\mathrm{e}} + \frac{\Delta \mathrm{Index}}{\Delta \log r}\ \log \frac{r}{r_{\mathrm{e}}} \equiv A - B \log \frac{r}{r_{\mathrm{e}}}, \quad (1)$$

where r is a projected radius and a suffix e indicates values defined at an effective radius r_{e}. When the line-strength

gradients were measured at different position angles, we use the effective radius r_e^* corrected for an eccentricity, as was done by DSP. Effective radii and eccentricities are taken from the original references, if available, and are supplementally taken from Davies et al. (1983), Djorgovski & Davis (1987), and Davies et al. (1987).

In general, linear regression lines give good approximations, but observed index values are systematically smaller at the inner most central parts and the outer regions beyond r_e. At galaxy centers with $\log r/r_e \lesssim -1.5$, the gradients are smeared out due to poor seeing conditions, and in the outer regions errors arising from the sky subtraction give poor fits. Therefore, we exclude these regions from our fitting. BS, DSP, CDB, CDa, and CDb all used the Lick indices (Burstein et al. 1984; Faber et al. 1985), while FFI and GON used Gonzalez's (1993) indices. However, differences are too small to affect the present analysis. CDB, DSP, CDa, CDb, and FFI converted spectral resolution of their measurements to Lick scales, but differences are negligible for Mg_2 and Mg_b which are our main concern.

Table 1 gives resulting fitting parameters of the line-strength gradients for 80 elliptical galaxies. Columns (1)-(7) gives a name of galaxy, reference, an index name, an intercept at r_e and error, a gradient and error, respectively. Mg_b is most suitable for a study of line-strength gradient, but the number of galaxies is not large enough to derive the statistics. The number of galaxies with the Mg_2 gradient data is largest in our sample. Fe_1 shows similar gradients to Mg_2, but Fe_2 shows a larger scatter, since it is very vulnerable to spectral resolutions and gradient of velocity dispersions. Therefore, we use Fe_1 instead of $\langle Fe\rangle = (Fe_1 + Fe_2)/2$, which was used in previous studies. Hβ is an age-sensitive index (Worthey 1994) and shows flat or positive gradients (DSP, GON, and FFI). A negative effect of Hβ emission may explain this (DSP), but this may be due to a decreasing stellar age towards a center of galaxy instead (GON, FFI). If the Hβ gradients reflect an age gradient within a galaxy, our old-age assumption for ellipticals is not correct anymore. The metallic line-strength gradients (Mg_2, Mg_b, Fe_1 and Fe_2) are all degenerate in age and metallicity, and a simple use of stellar population synthesis model in converting the line-strength gradients to the metallicity gradients would not be justified. We have solved the age-metallicity degeneracy by analyzing the absorption line gradients together with the Hβ gradients (section 2).

2.2. *Metallicity Gradients*

Since it is not certain whether all elliptical galaxies are equally old, we convert the line-strength gradients to the metallicity gradients in two alternative ways: (A) we assume that all ellipticals are 17 Gyr old and convert the indices to the metallicity, or (B) we assume that ellipticals are of different ages and the line-strength gradients reflect both the metallicity and age gradients. We have solved the age-metallicity degeneracy of the gradients by studying the Mg_2 and Hβ gradients simultaneously, but the number of galaxies to which Hβ data are available is small, and Hβ may be affected by the emission contamination. Therefore, we first calculate mean stellar metallicities of individual ellipticals under the assumption (A) and derive correlations between the mean stellar metallicity and other physical properties of galaxies. We then examine whether scatters of these correlations become smaller if we take into account a possible age effect under the assumption (B).

2.2.1. *Index-Metallicity Relations*

Under the assumption (A), the index-metallicity relations can be derived from spectral synthesis models. Comparing the relations given by seven different population synthesis models (Mould 1978; Peletier 1989; Buzzoni et al. 1992; Barbuy 1994; Worthey 1994; Casuso et al. 1996; Bressan et al. 1996), we find that, except Mould (1978) and Barbuy (1994), these models give very similar relations unless the metallicity is too low ([Fe/H] > -1). These relations are approximately given by the following form:

$$[\mathrm{Fe/H}] = p\ (\mathrm{Index}) - q. \tag{2}$$

Hereafter, we shall use the index-metallicity relations derived from Worthey's (1994) SSP models for 17 Gyr old galaxies:

$$\begin{aligned}
[\mathrm{Fe/H}] &= 5.85\ \mathrm{Mg_2} - 1.65,\\
[\mathrm{Fe/H}] &= 0.45\ \mathrm{Mg_b} - 1.87,\\
[\mathrm{Fe/H}] &= 0.67\ \mathrm{Fe_1} - 2.16,\\
[\mathrm{Fe/H}] &= 0.59\ \mathrm{Fe_2} - 1.77.
\end{aligned}$$

Quite often Mg_2 gives the [Fe/H] value ~ 0.2 dex higher than that derived from Fe_1. It may be due to our use of Worthey's model which assumes $[\alpha/\mathrm{Fe}] = 0$ for α elements such as oxygen, magnesium, silicon etc. We will discuss this in section 4.5. If we use Worthey's SSP models of 12 Gyr, we obtain systematically higher metallicities, but none of our main conclusions need to be modified.

If the metallic line-strength gradients are indeed reflecting the metallicity gradients, the observational data suggest that the gradients can be approximated in the following form:

$$[\mathrm{Fe/H}] = \log \frac{Z_e}{Z_\odot} - c \log \frac{r}{r_e}, \tag{3}$$

where $Z_\odot = 0.02$ is the solar metallicity and Z_e gives the stellar metallicity derived at $r = r_e$. A coefficient c gives the slope of metallicity gradient. On the other hand, from equations (1) and (2) we get the following equation:

$$[\mathrm{Fe/H}] = (Ap - q) - Bp\ \log \frac{r}{r_e}, \tag{4}$$

which gives the parameters Z_e and c in equation (3) for individual galaxies.

Figure 1 shows histograms of the line-strength gradients of the four indices, $-\Delta\mathrm{Mg_2}/\Delta\log r$, $-\Delta\mathrm{Mg_b}/\Delta\log r$, $-\Delta\mathrm{Fe_1}/\Delta\log r$, and $-\Delta\mathrm{Fe_2}/\Delta\log r$. Note that there is no sign of bimodality in the frequency distributions of the Mg_2, Mg_b, Fe_1, and Fe_2 gradients. This implies that, whatever the origin is, the gradients were formed by a single physical process. The average values are $\Delta[\mathrm{Fe/H}]/\Delta\log r = -0.30 \pm 0.12$ (Mg_2), -0.34 ± 0.16 (Mg_b), -0.28 ± 0.16 (Fe_1), and -0.25 ± 0.13 (Fe_2). All indices suggest that the metallicity gradients are in the range of $-0.6 \le \Delta[\mathrm{Fe/H}]/\Delta\log r \le -0.1$. A typical metallicity gradient is about $\Delta[\mathrm{Fe/H}]/\Delta\log r \sim -0.3$, which

is slightly steeper than the original estimate, because we have excluded the central regions where the gradients are significantly altered by poor seeings. The gradients thus derived are considerably flatter than a theoretical value -0.5 predicted by Carlberg (1984).

Figure 2 shows a frequency distribution of Mg_2 at the galaxy center, $(Mg_2)_0$, for 572 elliptical galaxies (dashed line) given by Davies et al. (1987), and 80 ellipticals (solid line) studied in this article. We note that there is no systematic difference between the two samples, thus we believe that we are dealing with a fairly good sample of elliptical galaxies in the local universe. Figure 3 gives frequency distributions of the four indices measured at the effective radius (i.e., the intercept at $r = r_e$). As we will see later (section 3), the metallicities evaluated at $r = r_e$ give good measures for the mean stellar metallicities. The average values are $\langle[Fe/H]\rangle = -0.18 \pm 0.19$ (Mg_2), -0.15 ± 0.24 (Mg_b), -0.37 ± 0.17 (Fe_1), and -0.36 ± 0.18 (Fe_2). Contrary to what Gonzalez & Gorgas (1996) claimed, the mean metallicities of ellipticals are not universal, but range from $\langle[Fe/H]\rangle \simeq -0.8$ to $+0.3$. A typical mean stellar metallicity of elliptical galaxies is about a half solar, $\langle[Fe/H]\rangle \simeq -0.3$, which is considerably smaller than the stellar metallicity $[Fe/H]_0 \simeq +0.2$ measured at the galaxy center. From a similar study of the Mg_2 gradients but with much smaller sample of ellipticals, Arimoto et al. (1997) found that the mean metallicity of typical elliptical galaxies with $\sigma_0 \geq 250$ km s^{-1} is $\langle[Fe/H]\rangle \simeq -0.06 \pm 0.13$. Our sample includes 19 ellipticals with $\sigma_0 \geq 250$ km s^{-1}, to which we obtain $\langle[Fe/H]\rangle \simeq -0.04 \pm 0.11$. Thus, a claim made by Arimoto et al. (1997) remains unexplained; i.e., the iron abundance of the interstellar mediums of luminous elliptical galaxies, as derived from ASCA X-ray observations of the iron L complex, is at variance with the abundance expected from the stellar populations as derived from current population synthesis methods of optical spectrum.

2.2.2. *Indices-Metallicity-Age Matrices*

Under the assumption (B), we find that the relations among two indices (one is Hβ and the other is either Mg_2 or Mg_b), age, and metallicity can be approximated with the following matrix forms:

$$\begin{pmatrix} \mathrm{Index}_1 \\ \mathrm{Index}_2 \end{pmatrix} = \begin{pmatrix} s_1 & s_2 \\ s_3 & s_4 \end{pmatrix} \begin{pmatrix} t_9 \\ [\mathrm{Fe/H}] \end{pmatrix} + \begin{pmatrix} q_1 \\ q_2 \end{pmatrix}, \quad (5)$$

$$\begin{pmatrix} t_9 \\ [\mathrm{Fe/H}] \end{pmatrix} = \begin{pmatrix} p_1 & p_2 \\ p_3 & p_4 \end{pmatrix} \begin{pmatrix} \mathrm{Index}_1 - q_1 \\ \mathrm{Index}_2 - q_2 \end{pmatrix}, \quad (6)$$

where t_9 is an age in units of Gyr. If we adopt Worthey's (1994) models, we obtain :

$$\begin{pmatrix} \mathrm{H}\beta \\ \mathrm{Mg}_2 \end{pmatrix} = \begin{pmatrix} -0.0425 & -0.607 \\ 0.00414 & 0.182 \end{pmatrix} \begin{pmatrix} t_9 \\ [\mathrm{Fe/H}] \end{pmatrix} + \begin{pmatrix} 2.12 \\ 0.211 \end{pmatrix},$$

$$\begin{pmatrix} t_9 \\ [\mathrm{Fe/H}] \end{pmatrix} = \begin{pmatrix} -34.9 & -116. \\ 0.792 & 8.12 \end{pmatrix} \begin{pmatrix} \mathrm{H}\beta - 2.12 \\ \mathrm{Mg}_2 - 0.211 \end{pmatrix},$$

$$\begin{pmatrix} \mathrm{H}\beta \\ \mathrm{Mg}_\mathrm{b} \end{pmatrix} = \begin{pmatrix} -0.0425 & -0.607 \\ 0.0583 & 2.28 \end{pmatrix} \begin{pmatrix} t_9 \\ [\mathrm{Fe/H}] \end{pmatrix} + \begin{pmatrix} 2.12 \\ 3.18 \end{pmatrix},$$

$$\begin{pmatrix} t_9 \\ [\mathrm{Fe/H}] \end{pmatrix} = \begin{pmatrix} -37.1 & -9.89 \\ 0.950 & 0.692 \end{pmatrix} \begin{pmatrix} \mathrm{H}\beta - 2.12 \\ \mathrm{Mg}_\mathrm{b} - 3.18 \end{pmatrix},$$

which are valid for $8 \lesssim t_9 \lesssim 17$ and $-0.5 \lesssim [Fe/H] \lesssim 0.5$ (see figure 4). With these equations, we can easily derive both metallicity gradient and age gradient simultaneously from the two line-strengths gradients. From equations (1) and (6), we obtain the following formal relations that give the age and metallicity gradients for individual galaxies:

$$t_9 = p_1(A_1 - q_1) + p_2(A_2 - q_2) - (p_1 B_1 + p_2 B_2)\ \log \frac{r}{r_e}, \quad (7)$$

$$[\mathrm{Fe/H}] = p_3(A_1 - q_1) + p_4(A_2 - q_2) - (p_3 B_1 + p_4 B_2)\ \log \frac{r}{r_e}, \quad (8)$$

where A_1, B_1 are for Index_1 and A_2, B_2 are for Index_2.

In applying these relations to individual elliptical, however, we find that resulting ages for several galaxies are not realistic (much larger than 17 Gyr old). This may probably due to a poor quality of Hβ gradient data. We therefore further assume that the age gradients are small and could be ignored. We only take into account a possibility that a whole stellar population of galaxy is systematically young, that is, we estimate a typical age of galaxy with an intercept of Hβ at the effective radius. Assuming no age gradients (i.e., $s_2 \sim 0, B_1 \sim 0$), we have derived the metallicity gradients by using the following equations for Mg_2 and Mg_b:

$$t_9 = (A_1 - q_1)/s_1, \quad (9)$$

$$[\mathrm{Fe/H}] = (A_2 - q_2 - s_3 t_9)/s_4 - B_2/s_4\ \log \frac{r}{r_e}. \quad (10)$$

3. MEAN STELLAR METALLICITY

It is well known that surface brightness profiles of elliptical galaxies are not fitted well with so-called de Vaucouleurs' law (Caon, Capacciolo, & D'Onofrio 1993; Binggeli & Jerjen 1997; Graham & Colless 1997). We, therefore, use Sersic law, which is a generalized de Vaucouleurs' law, by replacing a power index 1/4 with $1/n$. The parameter n correlates with a luminosity of a galaxy; a bright elliptical has $n = 4$ profile while a dwarf elliptical has exponential $n = 1$ profile (Binggeli & Jerjen 1997). In this section, we derive the mean stellar metallicity of an elliptical galaxy by using the observed line-strength gradients and the theoretical index - metallicity relations.

We assume that an elliptical galaxy is spherically symmetric and the surface brightness profile is given by Sersic law:

$$I(r) = I_e \exp\left[-b\left\{\left(\frac{r}{r_e}\right)^{\frac{1}{n}} - 1\right\}\right], \quad (11)$$

$$I_e = \frac{1}{2n\pi e^b b^{-2n}\Gamma(2n)} \frac{L_*}{r_e^2}, \quad (12)$$

where r is the projected radius and r_e is de Vaucouleurs' effective radius. b is a function of n determined from the definition of the effective radius and $b(n)$ is approximately given by the following equation:

$$b(n) = -0.326463 + 1.99927\ n. \quad (13)$$

The luminosity within the radius r is given by:

$$L(r) = \int_0^r 2\pi r I(r) dr = 2n\pi e^b b^{-2n} r_e^2 I_e\ \Gamma\left(2n, 0, b\left(\frac{r}{r_e}\right)^{\frac{1}{n}}\right), \quad (14)$$

where Γ is the general Gamma function. The total luminosity is given by:

$$L(\infty) = 2n\pi e^b b^{-2n}\Gamma(2n) r_{\rm e}^2 I_{\rm e} = L_*. \quad (15)$$

If we assume that the projected metallicity distribution is given by an exponential form, as the observed Mg_2 gradients suggest:

$$\bar{Z}(r) = Z_{\rm e}\left(\frac{r}{r_{\rm e}}\right)^{-c}, \quad (16)$$

the metallicity gradient is then given as:

$$[{\rm Fe/H}] = \log \bar{Z}(r) = \log\frac{Z_{\rm e}}{Z_\odot} - c\log\frac{r}{r_{\rm e}},$$

which is the same as equation (3). The parameters c and $Z_{\rm e}$ are determined from the parameters A and B in equation (1) and the index-metallicity relations are given by equation (8), or equations (4) and (10).

In an analogy to the surface brightness of stars, the *surface brightness profile of metals* can be defined as:

$$I_Z(r) = \bar{Z}(r) I(r). \quad (17)$$

Then the *luminosity of metals* within the radius r is given by:

$$L_Z(r) = \int_0^r 2\pi r I_Z(r) dr = b^{cn}\frac{\Gamma\left(2n - cn, 0, b\left(\frac{r}{r_{\rm e}}\right)^{\frac{1}{n}}\right)}{\Gamma\left(2n, 0, b\left(\frac{r}{r_{\rm e}}\right)^{\frac{1}{n}}\right)} Z_{\rm e} L_*. \quad (18)$$

The *total luminosity of metals* is given as follows:

$$L_Z(\infty) = b^{cn}\frac{\Gamma(2n-cn)}{\Gamma(2n)} Z_{\rm e} L_* \simeq Z_{\rm e} L_*, \quad (19)$$

where we note that the constant $b^{cn}\Gamma(2n-cn)/\Gamma(2n)$ is nearly equal to unity as is shown below.

If we assume that a mass-to-light ratio M/L is constant within a galaxy, the total mass of metals contained in stars can be given as:

$$M_Z(\infty) = b^{cn}\frac{\Gamma(2n-cn)}{\Gamma(2n)} Z_{\rm e} M_* \simeq Z_{\rm e} M_*, \quad (20)$$

where M_* is the total mass of stars in a galaxy. Finally the mean stellar metallicity can be given by:

$$\langle Z\rangle \equiv M_Z(\infty)/M^* = b^{cn}\frac{\Gamma(2n-cn)}{\Gamma(2n)} Z_{\rm e} \simeq Z_{\rm e}. \quad (21)$$

Although equation (21) gives an excellent measure for the mean stellar metallicity of elliptical galaxy, we hereafter use an explicit definition to calculate $\langle[{\rm Fe/H}]\rangle$ in such a way that we can take into account observed scatters of the metallicity gradients:

$$\langle[{\rm Fe/H}]\rangle = \log\left[b^{cn}\frac{\Gamma(2n-cn)}{\Gamma(2n)}\frac{Z_{\rm e}}{Z_\odot}\right]. \quad (22)$$

In table 2, we give the metallicity gradient parameters for 80 elliptical galaxies derived under the assumption (A) (hereafter, unless otherwise mentioned, all metallicities are calculated under the assumption (A)). Columns (1)-(2) give the name of galaxy and the reference. Columns (3)-(4), (5)-(6), (7)-(8) and (9)-(10) give the metallicity $Z_{\rm e}$ measured at the effective radius and the gradient c derived from Mg_2, $Mg_{\rm b}$, Fe_1, and Fe_2 gradients, respectively. Columns (11)-(15) give the mean metallicities derived from the Mg_2, $Mg_{\rm b}$, Fe_1, and Fe_2 gradients, respectively.

A typical elliptical galaxy has $n = 4$ and $c \sim 0.3$ (Figure 1), to which the constant $b^{cn}\Gamma(2n-cn)/\Gamma(2n)$ in equation (21) becomes $\simeq 1.1$, thus the mean metallicity of galaxy is very close to the metallicity measured at the effective radius. Arimoto et al. (1997) already showed that this is the case for smaller sample of galaxies if de Vaucouleurs' surface brightness profile is assumed. In this study, we have generalized it to Sersic's surface brightness profile and have found that so far as the slope c is smaller than 0.4, as is the case for most ellipticals, the mean metallicity is approximately given by $Z_{\rm e}$, which is smaller than the true mean by at most ~ 0.15 dex. $Z_{\rm e}$ values estimated by the Mg_2-, $Mg_{\rm b}$-, Fe_1-, and Fe_2-gradient are given in table 2.

Table 3a gives the mean metallicities for 12 ellipticals derived from the Mg_2 gradients under the assumption (B). Hβ corrections are explicitly taken into account. Columns (1)-(2) give the name of galaxy and the reference. Columns (3),(5), and (8) give the mean metallicities calculated from different equations as are indicated on the top line of the table; i.e., column (3) gives $\langle[{\rm Fe/H}]\rangle$ without any age gradient corrections, column (5) gives $\langle[{\rm Fe/H}]\rangle$ with constant age corrections, and column (8) gives $\langle[{\rm Fe/H}]\rangle$ with age gradient corrections, respectively. Column (4) gives a typical age $(t_9)_{\rm e}$ estimated from the intercept of Hβ at the effective radius by using equation (9). Columns (6)-(7) are parameters of the age gradients, the intercept $(t_9)_{\rm e} = p_1(A_1 - q_1) + p_2(A_2 - q_2)$ at the effective radius and the gradient $\Delta t_9 = -(p_1 B_1 + p_2 B_2)$, both calculated with equation (7). For individual galaxies, $\langle[{\rm Fe/H}]\rangle$ given in columns (5) and (8) are nearly identical, thus the age gradient correction is not crucial for deriving $\langle[{\rm Fe/H}]\rangle$. For NGC4278, NGC4486, NGC5636, NGC4839, and NGC7626 we obtain unexpectedly large Δt_9. This is probably because the Hβ gradients are contaminated by the emission components. We note that $\langle[{\rm Fe/H}]\rangle$ given in column (3) are not much different from those given in columns (5) and (8). Therefore, we conclude that the age corrections for $\langle[{\rm Fe/H}]\rangle$ are not important. Table 3b is the same as table 3a, but for 31 ellipticals with the $Mg_{\rm b}$ gradients. The same is true for $\langle[{\rm Fe/H}]\rangle$ given in table 3b. Except for 16 galaxies to which both equations (10) and (8) give unreasonable ages and age gradients, the resulting $\langle[{\rm Fe/H}]\rangle$ given in columns (3), (5), and (8) are nearly the same.

4. GLOBAL SCALING RELATIONS

Gonzalez & Gorgas (1996) claimed that elliptical galaxies with larger $(Mg_2)_0$ tend to have steeper Mg_2 gradients. They therefore suggested that the mass-metallicity relation of elliptical galaxies holds only for the central metallicity and claimed that the mean metallicity of elliptical galaxies should be universal. Since the mass-metallicity relation, or equivalently the color-magnitude relation, of

elliptical galaxies has been a fundamental relation that any theory of galaxy formation should account for (e.g., Arimoto & Yoshii 1987; Kodama & Arimoto 1997; Kauffmann & Charlot 1998), it is important to verify if mean stellar metallicities of ellipticals correlate tightly with other global properties, including luminosities, or if the mean metallicities are just universal for all ellipticals, regardless of their masses.

Table 4 gives physical properties of 80 elliptical galaxies: Columns (1)-(3) gives the name of galaxy, the reference, and the morphology type taken from RC3, respectively. Columns (4)-(8) gives the central Mg_2 index (mag), the central velocity dispersion (km s^{-1}), both are taken from Davies et al. (1987), the absolute effective radius (kpc), the absolute magnitude in B-band (mag), and $\kappa_1 = (\log \sigma_0^2 + \log R_e)/\sqrt{2}$ introduced by Bender, Burstein & Faber (1992) as a galaxy mass tracer, respectively. The effective radius and the absolute magnitude are calculated from Burstein et al. (1987) with the distance modulus estimated from the $D_n - \sigma$ relation of elliptical galaxies by C.Ikuta & N.Arimoto (private communications).

In the following arguments, we use if necessary, a ratio of the rotational velocity to a velocity dispersion $(v/\sigma)^*$, a parameter a_4 which shows the distortion of the isophotal contour (Bender et al. 1993), a parameter Σ which shows the kinematical peculiarity (Schweizer & Seitzer 1992), and a gas mass $M_{\rm gas}$ which is estimated from the *ASCA* X-ray observations (Matsushita 1997).

In the following sections, we demonstrate the global scaling relations for elliptical galaxies. Table 5 gives a result of our attempts for searching the relations. Columns (3) gives the number of galaxies used, and column (4) gives the correlation coefficient. The scaling laws are given in column (5) if the correlation coefficients are appreciably significant.

4.1. *Gradients versus Mean Metallicity*

In figures 5a and 5b, we plot the Mg_2 gradient against $[Fe/H]_0$ and $\langle[Fe/H]\rangle$, respectively. Contrary to what claimed by Gonzalez & Gorgas (1996), figures 5a and 5b show no evidence for any correlation. A study of Mg_b gradients concludes the same, although not shown here.

4.2. *Gradients versus Mass*

Figure 6a-6d show the Mg_2 gradient against galaxy mass tracers; the central velocity dispersion σ_0, the absolute B-magnitude M_B, the absolute effective radius R_e, and $\kappa_1 = (\log \sigma_0^2 + \log R_e)/\sqrt{2}$. Contrary to a prediction of numerical simulation (Carlberg 1984), figures 6 shows no evidence for any correlation.

4.3. *Metallicity-Mass Relation*

The color-magnitude relation of elliptical galaxies is usually interpreted as that luminous galaxies have higher mean stellar metallicities (Arimoto & Yoshii 1987; Kodama & Arimoto 1997). Figures 7a and 7c show how $\log \sigma_0$ correlates with $[Fe/H]_0$ and $\langle[Fe/H]\rangle$, respectively. Both are derived from Mg_2. The $\langle[Fe/H]\rangle$ - $\log \sigma_0$ relation is well defined and has nearly the same slope to that of the $[Fe/H]_0$ - $\log \sigma_0$ relation, but is systematically 0.3 dex lower; i.e., the mean stellar metallicity is about a half of the central metallicity. We note that the age correction by using Hβ changes little this relation. Figure 7b shows an equivalent relation derived from Mg_b. Although the slope is similar to that defined by Mg_2, the scatters are quite large. Figures 7d-7f are the same as figure 7c, but for the other mass tracers; M_B, R_e, and κ_1, respectively. We can also find a similar metallicity-mass relation for κ_1 with a little larger scatter, and in the case of M_B and R_e scatters become quite larger. This is because the relation with M_B and R_e is a face-on view of the fundamental plane, which we discuss in section 4.4. Therefore, we conclude that the metallicity-mass relation of ellipticals hold not only for the galaxy center but also for the whole stellar populations within a galaxy. When we use the mean metallicity with the correction of age estimated by Hβ in Table 3a and 3b, the scatters in the metallicity-mass relations do not become smaller.

4.4. *Fundamental Plane of Metallicity-Mass-Surface Brightness*

A fundamental plane (FP) is a correlation of elliptical galaxies with $2+n$ parameters (e.g., Djorgovski & Davies 1987; Dressler et al. 1987) and is a clue to understand formation and evolution of elliptical galaxies. One possible interpretation of the FP, defined by central velocity dispersions σ_0, absolute effective radii R_e, and surface brightnesses within an effective radius SB_e attributes it to a correlation of the mass-to-light ratio M/L to the total luminosity, or equivalently, to the total galaxy mass (e.g., Faber et al. 1987). The FP is observed up to $z \sim 0.5$ by recent HST observations (Kelson et al. 1997), which can be understood as an evidence for passive evolution of cluster elliptical galaxies since $z < 0.5$. The FP can be defined for colors or $(Mg_2)_0$ instead of σ_0 (de Carvalho & Djorgovski 1989). As we have seen above, $\langle[Fe/H]\rangle$ correlates well to σ_0. Therefore, we study if $\langle[Fe/H]\rangle$ defines new FPs with other global scaling properties. Table 6 gives the FPs of our sample; the first four are already well known FPs and the last two are the new FPs found in this study. Figures 7d and 7e ($\langle[Fe/H]\rangle$ against M_B and R_e, respectively) include significant scatters, which is because these figures are the face-on view of the FPs ($\langle[Fe/H]\rangle$, SB_e, and M_B or R_e). Even if we include a parameter SB_e to the $\langle[Fe/H]\rangle - \log \sigma_0$ relation (Figure 7c), we cannot reduce the scatter, which means figure 7c provides the exact edge-on view of the FP.

Figure 8 shows a new fundamental plane defined by $\langle[Fe/H]\rangle$, R_e, and SB_e. We interpret it as the correlation of the *metal mass-to-light ratio* M_z/L to the total luminosity. The FP of $\sigma_0 - SB_e - R_e$ is given by:

$$\sigma_0 \propto R_e^{0.64} \langle\Sigma\rangle_e^{0.68}. \tag{23}$$

The FP of $\langle[Fe/H]\rangle - SB_e - R_e$ is:

$$\langle Z\rangle \propto R_e^{1.26} \langle\Sigma\rangle_e^{1.38}. \tag{24}$$

With the definition of the surface brightness $\langle\Sigma\rangle_e \equiv 2L/\pi R_e^2$ ($SB_e \equiv -2.5\log\langle\Sigma\rangle_e$), the virial theorem $GM/R_e \propto \sigma_0^2$, and the definition of metallicity $M_Z/M \equiv \langle Z\rangle$, we get the following equations:

$$M/L \propto R_e^{-0.42} L^{0.35}. \tag{25}$$

$$M_Z/L \propto R_{\rm e}^{-1.91} L^{1.73}. \quad (26)$$

where L, M and M_Z are the luminosity, the mass, the mass of the metals of the galaxy, respectively.

4.5. *Magnesium Enrichment?*

It has been quite often claimed that magnesium and perhaps other α-elements are overabundant in central regions of elliptical galaxies (Worthey, Faber, & Gonzalez 1992; Davies et al. 1993; Gonzalez 1993; Fisher et al. 1995b). In particular, Fisher et al. (1995b) demonstrated that ellipticals with larger σ_0 tend to have larger $[{\rm Mg/Fe}]_0$ (c.f., Trager et al. 1998). We have studied if this is also true for the mean abundances of these elements.

Figure 9 compares $\langle[{\rm Fe/H}]\rangle$ given by Mg_2 and Fe_1, respectively. As is clearly seen, $\langle[{\rm Fe/H}]\rangle_{\rm Mg_2}$ are higher than $\langle[{\rm Fe/H}]\rangle_{\rm Fe_1}$ by ~ 0.2 dex. If Mg_2 and Fe_1 reflect the abundances of magnesium and iron, respectively, figures 9 implies that magnesium is enhanced by ~ 0.2 dex with respect to iron in everywhere within a galaxy. We have checked if there is any systematic difference in the gradients of Mg_2 and Fe_1, but fail to find any clear correlation. We do not find any relation between $\langle[{\rm Mg/Fe}]\rangle$ and dynamical or luminous masses, as shown in table 6. We also note that in figure 9 there is no trend of increasing $\langle[{\rm Mg/Fe}]\rangle$ towards higher $\langle[{\rm Fe/H}]\rangle_{\rm Mg_2}$; or in other words, $\langle[{\rm Mg/Fe}]\rangle \simeq +0.2$ in most elliptical galaxies independent of their mass, in contrast to what was claimed for $[{\rm Mg/Fe}]_0$. This can be seen much clearly in figures 10a-10d in which we plot $\langle[{\rm Mg/Fe}]\rangle$ against $\log\sigma_0$, M_B, $R_{\rm e}$, and κ_1, respectively. Obviously, these figures do not show any correlation at all.

However, a word of caution is to be given. The magnesium enhancement might not be real. Although Fe_1 is less fragile to the velocity dispersion gradient than Fe_2, the observational errors of Fe_1 are much larger than those of Mg_2. It is not yet fully understood whether Mg_2 gives [Mg/H] and Fe_1 traces [Fe/H]. Indeed, Mg_2 depends strongly on carbon, iron, and several other spices (Tripicco & Bell 1995). An increase of metallicity increases the opacity and changes the structure of stellar atmosphere, as a result of which the indices will be strengthened; thus Mg_2 should also be sensitive to [Fe/H]. Therefore, one should keep in mind that the ratio of Mg_2 to Fe_1 may not directly give the [Mg/Fe] ratio.

The point we wish to make here is as follows: Previously, it was claimed that more massive ellipticals tend to have [Mg/Fe] ratios (e.g., Fisher et al. 1995b). This claim based on the assumption that Mg_2 and Fe_1 give [Mg/H] and [Fe/H], respectively, and used only central values of Mg_2 and Fe_1 for their analyses. Under the same assumption, but if $\langle[{\rm Mg/H}]\rangle$ and $\langle[{\rm Fe/H}]\rangle$ are used instead, there exists no clear correlation between $\langle[{\rm Mg/Fe}]\rangle$ and the galaxy mass (figures 10a-10d). If the assumption we made turns out to be wrong, our conclusion should be wrong, but Fisher et al.'s (1995b) argument should also lose its standing point.

Magnesium is mainly produced by Type II supernovae (SNe II), while the bulk of iron is produced by Type Ia supernovae (SNe Ia), and SNe II and SNe Ia have different lifetimes; 10^{6-8} yr and a few Gyr, respectively (c.f., Kobayashi et al. 1998). Thus, the [Mg/Fe] ratio provides crucial constraints on the timescale of chemical enrichment in elliptical galaxies. Based on the previous findings for the ratio of Mg_2 and Fe_1 at the galaxy center, it has been suggested that the magnesium enhancement in elliptical galaxies can be explained (e.g., Worthey et al. 1992; Matteucci 1994), if 1) the duration of star formation is shorter than a few Gyr before SNe Ia start to explode, or if 2) a slope of initial mass function (IMF) is flatter than a slope of the Salpeter IMF to produce more SNe II, or if 3) the metal enriched wind induced the selective mass loss and ejected the iron enriched gas before it is consumed for forming next generations of stars (Vader 1986; 1987), or if 4) the binary frequency is smaller and produces less SNe Ia in ellipticals (Arimoto et al. 1997), or if 5) SNe Ia explode less frequently in metal rich environment, which is contrary to what is expected theoretically (Kobayashi et al. 1998), or if 6) the yields of SNe II significantly depend on the metallicity (Maeder 1992). In the present study, we find that $\langle[{\rm Mg/Fe}]\rangle \simeq +0.2$ regardless of the galaxy mass. This can be most naturally explained if the star formation had stopped in elliptical galaxies before the bulk of SNe Ia began to explode, as was already predicted by a galactic wind model by Arimoto & Yoshii (1987). A recent detailed study of metallicity effects on SNe Ia by Kobayashi et al. (1998) suggests that duration of the star formation in elliptical galaxies should be ~ 1 Gyr.

5. DISCUSSIONS

5.1. *Dispersion*

Global metallicities of elliptical galaxies correlate with central velocity dispersions but with rather large dispersions (figure 7c). This comes from the fact that the metallicity gradient of elliptical galaxies is not uniquely determined by the galaxy mass. Figure 11 shows three sequences of galaxies with various gradients. All galaxies are normal ellipticals showing no significant peculiarity. Left panel shows a sequence of $({\rm Mg_2})_{\rm e} = {\rm const.}$, so that these galaxies have the same intercepts at the effective radius and yet show different gradients. This means that elliptical galaxies can have the same mean metallicities even if the metallicities at the galaxy center are considerably different. Middle panel shows a sequence of $({\rm Mg_2})_0 = {\rm const.}$, thus these galaxies have the same central Mg_2, but have different gradients. This implies that even if the galaxy mass is the same, elliptical galaxies can have significantly different mean stellar metallicities. Right panel shows a sequence of $\Delta{\rm Mg_2}/\Delta\log r = {\rm const.}$, indicating that ellipticals can have the same Mg_2 gradient while global metallicities are different.

5.2. *Errors*

Non-negligible scatters observed in the $\langle[{\rm Fe/H}]\rangle$ - $\log\sigma_0$ relation (figure 7c) might arise from observational errors involved in the line-strength measurements and the velocity dispersions. To see if one can attribute the dispersion entirely to the observational errors, we evaluate the individual errors.

The effective radius $r_{\rm e}$ is sometimes difficult to determine, and in the worst case, $r_{\rm e}$ differs almost 10 arcsec from authors to authors (Fisher, Illingworth, & Franx 1995a). However, with $\Delta{\rm Mg_2}/\Delta\log r \simeq -0.051$, a change

brought into mean metallicities is Δ[Fe/H] ~ 0.05, thus is negligibly small.

It is not always the case to adopt the same spectral resolutions. The offset resulted from different resolutions is as large as $\Delta Mg_2 \sim 0.03$ and $\Delta Fe_1 \sim 0.5$. The resulting errors in $\langle$[Fe/H]$\rangle$ are $\Delta[Fe/H]_{Mg_2} \sim 0.2$ and $\Delta[Fe/H]_{Fe_1} \sim 0.3$, which could partly account for the dispersions, but not entirely.

Velocity dispersions in ellipticals usually decrease from the galaxy center to the outer area. The correction factors are 1.02 for Mg_2, 1.23 for Fe_1, and 1.5 for Fe_2 at the velocity dispersion $\sigma = 300$ km s^{-1}, which are negligible for the Mg_2 gradient, but are significant for the Fe_1 and Fe_2 gradients (Davies et al. 1993).

Some elliptical galaxies are known to have the surface brightness profile that deviates significantly from de Vaucouleurs' law (Caon et al. 1993; Binggeli & Jerjen 1997; Graham & Colless 1997). Therefore, we use Sersic law for the surface brightness profile and study how the resulting mean metallicity depends on the n parameter. We find that the effect of changing n is negligibly small.

Many ellipticals tend to have less steep gradients at the galaxy center. Although it is likely that this is caused by poor seeings, one may argue that it introduces errors in the resulting metallicity. However, the stellar mass involved within $\log r/r_e = -1.5$ is only $\sim 2\%$, and therefore the errors due to this effect should be small.

The mass-to-light ratio M/L differs from galaxy to galaxy (Faber & Jackson 1976; Michard 1980; Schechter 1980). This would affect the absolute magnitudes M_B, but not the velocity dispersions.

None of the observational errors can fully account for the large scatter in the $\langle$[Fe/H]$\rangle$ - $\log\sigma_0$ relation. Therefore, we conclude that the scatters in metallicity-mass relations are at least partly real.

5.3. *Mergers?*

To examine if this dispersion of the metallicity gradient and the scatter of metallicity-mass relations come from galaxy mergers, we check whether the metallicity gradients and the residuals from the ridge line of $\langle$[Fe/H]$\rangle$ - $\log\sigma_0$ relation correlate with dynamical disturbances, such as a ratio of rotational velocity to velocity dispersion $(v/\sigma)^*$, an isophotal contour deviation a_4, a dynamical peculiarity Σ, and the mass of hot X-ray gas M_{gas}. We fail to find any definite evidence suggesting that the dispersion of metallicity gradient, the scatter of metallicity-mass relations and the dynamical disturbances come from the same origin.

5.4. *Age Effects?*

Major results and conclusions of this article entirely depend on our assumption that line-strength gradients should be read as the metallicity gradients. The gradients of Mg_2, Mg_b, Fe_1, and Fe_2 may also arise from a gradient of age that decreases from the galaxy center to the outer halo. Indeed, in many cases Hβ shows a positive gradient, thus is consistent with the age gradient scenario. To estimate possible influences of the age gradient on our $\langle$[Fe/H]$\rangle$, we have assumed that the Mg_2 and Hβ gradients are caused by both metallicity and age, and have derived the age and metallicity gradients simultaneously (table 3a and 3b). Except for the cases in which we obtain unexpectedly large ages and/or age gradients, the resulting $\langle$[Fe/H]$\rangle$ are not much different from what we obtain with no age gradients, and the scatter of metallicity-mass relation is nearly the same even if age gradients are considered. However, Hβ is not a good age indicator, and until it becomes possible to analyze the gradients of new Hγ defined by Vazdekis & Arimoto (1999), one cannot exclude the possibility of age gradient conclusively.

Nevertheless, we wish to claim that the line-strength gradients are due to the metallicity gradient. Quite recently, Tamura et al. (1999) have measured gradients of HST V_{606}-I_{814} colors of 7 elliptical-like galaxies in the Hubble Deep Field (HDF); 2-456.0 (z=0.089), 2-121.0 (z=0.475), 3-790.0 (z=0.562), 3-321.0 (z=0.677), 4-744.0 (z=0.764), 4-493.0 (z=0.847), and 4-752.0 (z=1.013). These galaxies are red and their luminosity profiles follow de Vaucouleurs' law, thus it is very likely that they are genuine ellipticals. The V_{606}-I_{814} gradients of these galaxies do not show significant difference, and this means that the color gradients of ellipticals evolve passively since $z \simeq 1$. Tamura et al. (1999) build two evolutionary sequences of ellipticals by assuming that (a) the color gradients are entirely due to the metallicity gradient (a metallicity sequence) and (b) the color gradients arise from the age gradient (an age sequence). The color gradients of the metallicity sequence evolve passively and do not change significantly from the present to $z \simeq 1$. On the other hand, the color gradients of the age sequence become significantly steeper beyond $z \simeq 0.5$ and become almost vertical at $z \simeq 1$. Obviously, 7 ellipticals in the HDF do not agree with an evolution of the age sequence at all, but show quite excellent agreement with theoretical evolutionary loci of the metallicity sequence. Therefore, the color gradients of ellipticals certainly reflect the gradient of stellar metallicity. Then, why not the line-strength gradients?

6. CONCLUSIONS

We have re-studied line-strength gradients of 80 elliptical galaxies. Our sample galaxies show a very similar central $(Mg_2)_0$ distribution to that of 572 ellipticals studied by Davies et al. (1987). We assume that the gradients of metallic lines, such as Mg_2, Mg_b, Fe_1, and Fe_2, all originate from the gradient of mean stellar metallicity in elliptical galaxies, and have applied Worthey's (1994) index-metallicity relations to get Δ[Fe/H]$/\Delta\log r = -0.30\pm0.12$ (Mg_2), -0.34 ± 0.16 (Mg_b), -0.28 ± 0.16 (Fe_1), and -0.25 ± 0.13 (Fe_2) and find more than 80% of elliptical galaxies show the metallicity gradients in the range of $-0.6 \leq \Delta$[Fe/H]$/\Delta\log r \leq -0.1$. A typical gradient Δ[Fe/H]$/\Delta\log r \simeq -0.3$ is flatter than the gradients predicted by monolithic collapse simulations (Larson 1974a; Carlberg 1984). The metallicity gradients do not correlate with any physical properties of galaxies, including central and mean metallicities, central velocity dispersions σ_0 , absolute B-magnitudes M_B, absolute effective radii R_e, and dynamical masses of galaxies. Unless there are significant unknown errors in the measurements of line-strength gradients, elliptical galaxies have different metallicity gradients, even if they have nearly identical properties such as masses and luminosities. This rather surprising behavior of the line-strength gradients has never been taken into

account in modeling the formation of elliptical galaxies.

By using the metallicity gradients, we have calculated mean stellar metallicities for individual ellipticals. The average metallicities of our sample are $\langle[\mathrm{Fe/H}]\rangle = -0.18 \pm 0.19$ ($\mathrm{Mg_2}$), -0.15 ± 0.24 ($\mathrm{Mg_b}$), -0.37 ± 0.17 ($\mathrm{Fe_1}$), and -0.36 ± 0.18 ($\mathrm{Fe_2}$), and a typical metallicity is a half solar, $\langle[\mathrm{Fe/H}]\rangle \simeq -0.3$. Contrary to what Gonzalez & Gorgas (1996) claimed, the mean metallicities of ellipticals are not universal, but range from $\langle[\mathrm{Fe/H}]\rangle \simeq -0.8$ to $+0.3$. Since the mean metallicity of 19 elliptical galaxies with $\sigma_0 \geq 250$ km s^{-1} is $\langle[\mathrm{Fe/H}]\rangle \simeq -0.04 \pm 0.11$, a claim made by Arimoto et al. (1997) remains unexplained; i.e., the iron abundance of the interstellar mediums of luminous elliptical galaxies, as derived from ASCA X-ray observations of the iron L complex, is at variance with the abundance expected from the stellar populations. $\langle[\mathrm{Fe/H}]\rangle$ correlates well with σ_0 and dynamical mass, though relations for M_B and R_e include significant scatters. We find the fundamental planes defined by surface brightnesses SB_e, $\langle[\mathrm{Fe/H}]\rangle$, and R_e (or M_B), the scatters of which are much smaller than those of the $\langle[\mathrm{Fe/H}]\rangle$ - R_e (or M_B) relation. The $\langle[\mathrm{Fe/H}]\rangle$ - $\log\sigma_0$ relation is nearly in parallel to the $[\mathrm{Fe/H}]_0$ - $\log\sigma_0$ relation but systematically lower by 0.3 dex; thus the mean metallicities are about a half of the central values. The metallicity-mass relation, or equivalently, the color-magnitude relation of ellipticals holds not only for the central part but also for the whole part of galaxies.

Assuming that $\mathrm{Mg_2}$ and $\mathrm{Fe_1}$ give [Mg/H] and [Fe/H], respectively, we find $\langle[\mathrm{Mg/Fe}]\rangle \simeq +0.2$ in most of elliptical galaxies. $\langle[\mathrm{Mg/Fe}]\rangle$ shows no correlation with galaxy mass tracers such as σ_0, in contrast to what was claimed for the central [Mg/Fe]. This can be most naturally explained if the star formation had stopped in elliptical galaxies before the bulk of SNe Ia began to explode.

Elliptical galaxies can have significantly different metallicity gradients and $\langle[\mathrm{Fe/H}]\rangle$ even if they have the same galaxy mass. This may result from different history of galaxy mergers, as suggested by White's (1980) simulation. However, we fail to find any evidence suggesting the same origin for the dispersion of metallicity gradient, the scatter around the metallicity-mass relation, and the dynamical disturbances; none of available data of Σ, a_4, and $(v/\sigma)^*$ show a correlation with the gradients and the scatters. The scatters of both gradient and metallicity-mass relation might come from dust obscuration, but contrary to broad band colors, line strengths are far less sensitive to the dust. Another possibility is that the scatters are due to different ages and age gradients. However, the scatters are affected little by the age and age gradient which we derive from H_β, although H_β may not be a good age indicator. If it turns out that these galaxies are old and have no peculiar age gradients, the scatters discussed in this paper should have their origin at the formation epoch of galaxies.

We would like to express our heartfelt thanks to our anonymous referee whose critical reading of our draft improved significantly the paper. We are grateful to C.M.Carollo, J.Gorgas, and R.P.Saglia for providing us the machine readable data of their line-strength gradients. We thank to T.Yamada, K.Ohta and N.Tamura for fruitful discussions. C.K. thanks to the Japan Society for Promotion of Science for a finantial support. This work was financially supported in part by a Grant-in-Aid for the Scientific Research (No.0940311) by the Japanese Ministry of Education, Culture, Sports and Science.

APPENDIX

$\mathrm{MG_2}$ AND $\mathrm{MG_B}$ GRADIENTS OF EARLY-TYPE GALAXIES

To give a comprehensive view of the line-strength gradients, we show in figures 12 and 13 the $\mathrm{Mg_2}$ and $\mathrm{Mg_b}$ gradients of 133 early-type galaxies including compact ellipticals, S0 galaxies, and bulge of spirals. Filled circles and crosses are the observational data taken from F77, EG, CH, PEL, GEA, BT, D91a, D91b, BS, D92, CDB, DSP, GON, HP, SAG, CDa, CDb, SPD, CGA, and FFI. We plot the data taken along several position angles, after correcting for the eccentricity. Solid lines give regression lines which are calculated by using only filled circles.

REFERENCES

Arimoto, N., Matsushita, K., Ishimaru, Y., Ohashi, T., & Renzini, A. 1997, ApJ, 477, 128
Arimoto, N., & Yoshii, Y. 1987, A&A, 173, 23
Barbuy, B. 1994, ApJ, 430, 218
Baugh, C.M., Cole, S., Frenk, C.S., & Lacey, C.G. 1997, ApJ, 498, 504
Bender, R., Burstein, D., & Faber, S.M. 1992, ApJ, 399, 462
Bender, R., Burstein, D., & Faber, S.M. 1993, ApJ, 411, 153
Bender, R., & Surma, P. 1992, A&A, 258, 250
Binggeli, B., & Jerjen, H. 1998, A&A, 333, 17
Boroson, T.A., & Thompson, I.B. 1991, AJ, 101, 111
Bower, R.G., Lucey, J.R., & Ellis, R.S. 1992, MNRAS, 254, 601
Bressan, A., Chiosi, C., & Tantalo, R. 1996, A&A, 311, 425
Burstein, D. 1979, ApJ, 232, 74
Burstein, D., Daveis, R.L., Dressler, A., Faber, S.M., Lynden-Bell, D., Terlevich, R., & Wegner, C. 1988, in Towards Understanding Galaxies at Large Redshift, ed. R.G. Kron & A. Renzini (Dordrecht:Kluwer), p.17
Burstein, D., Davies, R.L., Dressler, A., Faber, S.M., Stone, R.P.S., Lynden-Bell, D., Terlevich, R., & Wegner, C. 1987, ApJS, 64, 601
Burstein, D., Faber, S.M., Gaskell, C.M., & Krumm, N. 1984, ApJ, 287, 586
Butcher, H.R., & Oemler, A. 1978, ApJ, 219, 18
Butcher, H.R., & Oemler, A. 1984, ApJ, 285, 426
Buzzoni, A., Gariboldi, G., & Mantegazza, L. 1992, AJ, 103, 1814
Caon, N., Capacciolo, M., & D'Onofrio, M. 1993, MNRAS, 265, 1013
Cardiel, N., Gorgas, J., & Aragón-Salamanca, A. 1995, MNRAS, 277, 502
Carlberg, R.G. 1984, ApJ, 286, 403
Carollo, C.M., & Danziger, I.J. 1994a, MNRAS, 270, 523
Carollo, C.M., & Danziger, I.J. 1994b, MNRAS, 270, 743
Carollo, C.M., Danziger, I.J., & Buson, L. 1993, MNRAS, 265, 553
Casuso, E., Vazdekis, A., Peletier, R.F., & Beckman, J.E. 1996, ApJ, 458, 533
Ciotti, L., D'Eecole, A., Pellegrini, S., & Renzini, A. 1991, ApJ, 376, 380
Cole, S., Aragón-Salamanca, A., Frenk, C.S., Navarro, J.F., & Zepf, S.E. 1994, MNRAS, 271, 781
Couture, J., & Hardy, E. 1988, AJ, 96, 867
Davies, R.L., Burstein, D., Dressler, A., Faber, S.M., Lynden-Bell, D., Terlevich, R.J., & Wegner, G. 1987, ApJS, 64, 581

Davies, R.L., Efstathiou, G., Fall, S.M., Illingworth, G., & Schechter, P.L. 1983, ApJ, 266, 41
Davies, R.L., & Sadler, E.M. 1987, in IAU Symp. 127, Structure and Dynamics of Elliptical Galaxies, ed. T. de Zeeuw (Dorderecht: Reidel), p.441
Davies, R.L., Sadler, E.M., & Peletier, R.F. 1993, MNRAS, 262, 650
Davidge, T.J. 1991a, AJ, 101, 884
Davidge, T.J. 1991b, AJ, 102, 896
Davidge, T.J. 1992, AJ, 103, 1512
de Carvalho, R.R., & Djorgovski, S. 1989, ApJ, 341, L37
Dickinson, M. 1996, in ASP Conference Series, 86, Fresh Views of Elliptical Galaxies, eds., A.Buzzoni, A.Renzini, & A.Serrano, p.283
Djorgovski, S., & Davis, M. 1987, ApJ, 313, 59
Dressler, A. 1980, ApJ, 236, 351
Dressler, A. 1984, ApJ, 281, 512
Dressler, A., & Gunn, J.E. 1983, ApJ, 270, 7
Dressler, A., & Gunn, J.E. 1992, ApJS, 78, 1
Dressler, A., Lynden-Bell, D., Burstein, D., Davies, R.L., Faber, S.M., Terlevich, R.J., & Wegner, G. 1987, ApJ, 313, 42
Dressler, A., Oemler, A., Couch, W.J., Smail, I., Ellis, R.S., Barger, A., Butcher, H., Poggianti, B.M., & Sharples, R.M. 1997, ApJ, 490, 577
Driver, S.P., Windhorst, R.A., & Griffiths, R.E. 1995, ApJ, 453, 48
Efstathiou, G., & Gorgas, J. 1985, MNRAS, 215, 37
Faber, S.M. 1973, ApJ, 179, 731
Faber, S.M. 1977, in The Evolution of Galaxies and Stellar Populations, eds., B.M.Tinsley, R.B.Larson (New Heaven: Yale Univ. Press), p.157
Faber, S.M., Dressler, A., Davies, R.L., Burstein, D., Lynden-Bell, D., Terlevich, R., & Wegner, G. 1987, in Nearly Normal Galaxies, From the Planck Time to the Present, ed. S.M.Faber (NY: Springer), p.175
Faber, S.M., Friel, E.D., Burstein, D., & Gaskell, C.M. 1985, ApJS, 57, 711
Faber, S.M., & Jackson, R.E. 1976, ApJ, 204, 668
Fisher, D., Franx, M., & Illingworth, G. 1995b, ApJ, 448, 119
Fisher, D., Illingworth, G., & Franx, M. 1995a, ApJ, 438, 539
Forbes, D.A., Brodie, J.P., & Grillmair, C.J. 1997, AJ, 113, 1652
Franceschini, A., Silva, L., Fasano, G., Granato, G. L., Bressan, A., Arnouts, S. & Danese, L. 1998, ApJ, 506, 600
Franx, M., & Illingworth, G. 1990, ApJ, 359, L41
Franx, M., Kelson, D., van Dokkum, P., Illingworth, G., Fabricant, D. 1996, in Galaxy Scaling Relations, Origins, Evolution and Applications, eds. L.N. Da Costa, A.Renzini, Springer-Verlag, p.185
Gonzalez, J.J. 1993, PhD thesis, Univ. of Califolnia
Gonzalez, J.J., & Gorgas, J. 1996, in ASP Conference Series, 86, Fresh Views of Elliptical Galaxies, eds., A.Buzzoni, A.Renzini, & A.Serrano, p.225
Gorgas, J., Efstathiou, G., & Aragón-Salamanca, A. 1990, MNRAS, 245, 217
Graham, A., & Colless, M. 1997, MNRAS, 287, 221
Harris, W.E. 1991, ARA&A, 29, 543
Hes, R., & Peletier, R.F., 1993, A&A, 268, 539
Kauffmann, G., & Charlot, S. 1998, MNRAS, 294, 705
Kauffmann, G., & White, S.D.M. 1993, MNRAS, 261, 921
Kelson, D.D., van Dokkum, P.G., Franx, M., Illingworth, G.D., & Fabricant, D. 1997, ApJ, 478, L13
Kobayashi, C., Tsujimoto, T., Nomoto, K., Hachisu, I, & Kato, M. 1998, ApJ, 503, L155
Kodama, T., & Arimoto, N. 1997, A&A, 320, 41
Kodama, T., & Arimoto, N. 1998, MNRAS, 300, 193
Kodama, T., Arimoto, N., Barger, A.J., & Aragón-Salamanca, A. 1998a, A&A, 334,99
Kodama, T., Bower, R.G., & Bell, E.F. 1998b, astro-ph/9810138
Kormendy, J., & Djorgovski, S. 1989, ARA&A, 27, 235
Larson, R.B. 1974a, MNRAS, 166, 585
Larson, R.B. 1974b, MNRAS, 169, 229
Larson, R.B. 1975, MNRAS, 173, 671
Maeder, A. 1992, A&A, 264, 105
Matsushita, K. 1997, PhD thesis, Univ, of Tokyo
Matteucci, F. 1994, A&A, 288, 57
Michard, R. 1980, A&A, 91, 122
Mould, J.R. 1978, ApJ, 220, 434
Ostriker, J. 1980, Comments on Astrophysics, 8, 177
Peletier, R.F., 1989, PhD thesis Univ. of Groningen
Saglia, R.P., Bertin, G., Bertola, F., Danziger, J., Dejonghe, H,, Sadler, E.M., Stiavelli, M., de Zeeuw, P.T., & Zeilinger, W.W. 1993, ApJ, 403, 567
Sansom, A.E., Peace, G., & Dodd, M. 1994, MNRAS, 271, 39
Schade, D., Barrientos, L.F., & Lopez-Cruz, O. 1997, ApJ, 477, L17
Schechter, P.L. 1980, AJ, 85, 801
Schweizer, F., & Seitzer, P. 1992, AJ, 104, 1039
Schweizer, F., Seitzer, P., Faber, S.M., Burstein, D., Ore, C.M.D., & Gonzalez, J.J. 1990, ApJ, 364, L33
Stanford, S.A., Eisenhardt, P.R.M., & Dickinson, M. 1998, ApJ, 492, 461
Tamura, N, Kobayashi, C., Arimoto, N., Ohta, K., & Kodama, T 1999, in preparation
Terlevich, R., Davies, R.L., Faber, S.M., & Burstein, D. 1981, MNRAS, 196, 381
Toomre, A. & Toomre, J. 1972, ApJ, 178, 623
Trager, R.C., Worthey, G., Faber, S.M., Burstein, D. & Gonzlez, J.J. 1998, ApJS, 116, 1
Tripicco, M.J. & Bell, R.A. 1995, AJ, 110, 3035
Vader, J.P. 1986, ApJ, 305, 669
Vader, J.P. 1987, ApJ, 317, 128
van den Bergh, S. 1982, PASP, 94, 459
van den Bergh, S. 1990, in Dynamics and Interaction of Galaxies, ed., R. Wielen (Berlin:Springler), p.492
Vazdekis, V.A. & Arimoto, N. 1999, ApJ, in press (astro-ph/9906140)
White, S.D.M. 1980, MNRAS, 191, 1p
Whitmore, B.C., & Schweizer, F. 1995, AJ, 109, 960
Worthey, G. 1994, ApJS, 95, 107
Worthey, G., Faber, S.M., & Gonzalez, J.J. 1992, ApJ, 398, 69

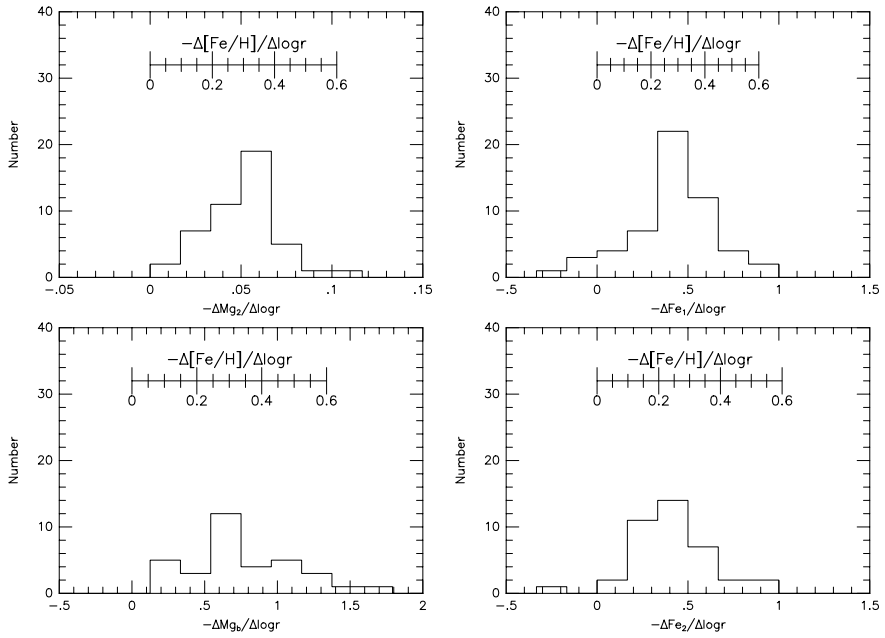

FIG. 1.— The frequency distributions of the line-strength gradients. From the upper-left to the lower-left in clockwise, the panels show Mg_2, Fe_1, Fe_2, and Mg_b, respectively. The metallicity scales are taken from the index-metallicity relations of Worthey's (1994) population synthesis models, provided that galaxies are 17 Gyr old.

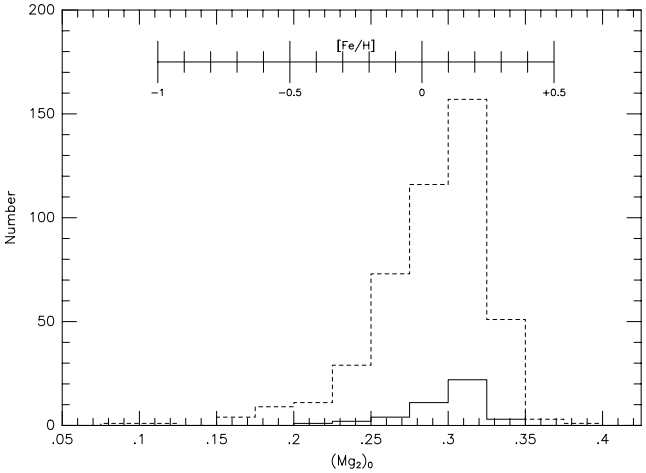

FIG. 2.— The frequency distribution of Mg_2 at a galaxy center for 572 ellipticals (dashed line) taken from Davies et al. (1987) and 46 ellipticals of our sample (solid line). The metallicity scale is the same as in figure 1.

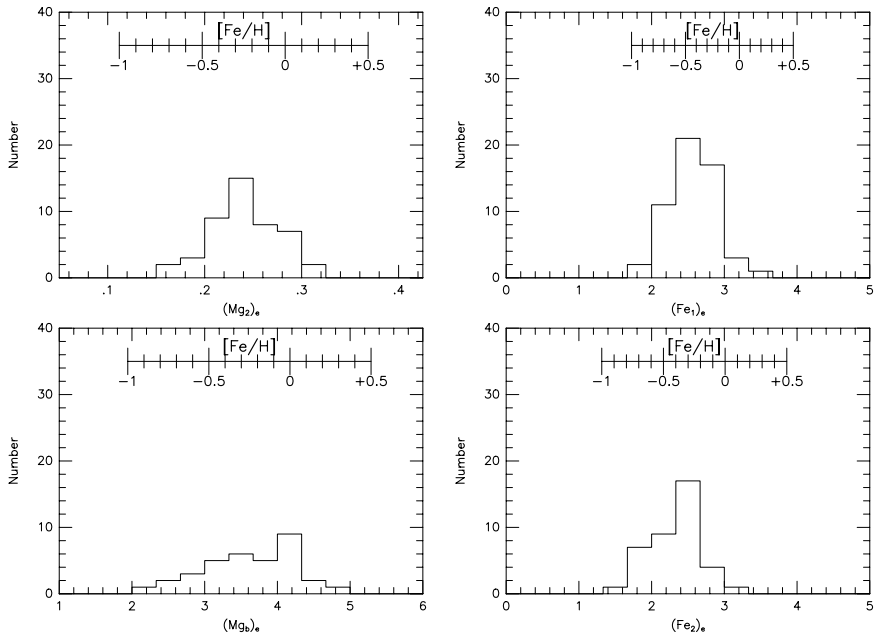

FIG. 3.— The same as figure 1, but for the intercepts at the effective radius.

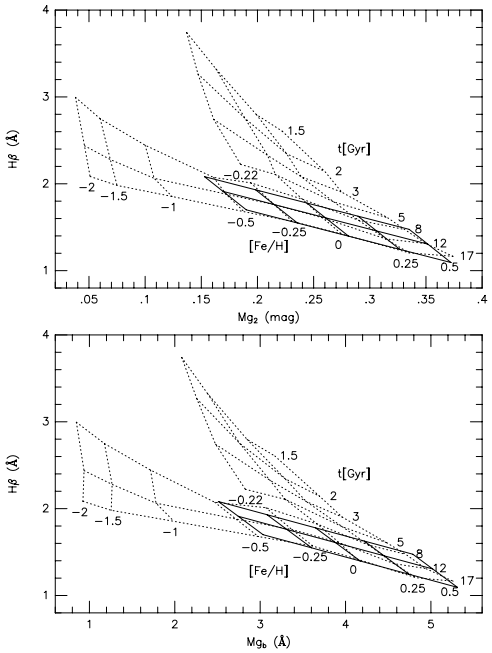

FIG. 4.— Hβ versus Mg_2 (upper panel) and Mg_b (lower panel) relations as a function of age and metallicity. Dotted lines give simple stellar population models of Worthey (1994), and solid lines are the approximated relations adopted in this paper.

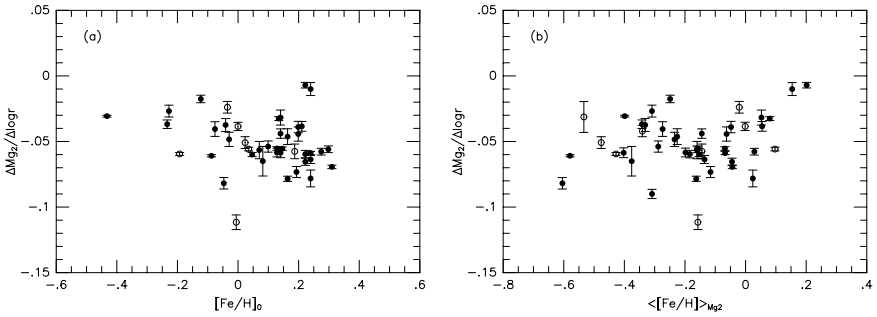

FIG. 5.— The Mg_2 gradient versus the metallicity. Open and filled circles show cD and elliptical galaxies, respectively. (a) and (b) are for the central metallicity, and the mean stellar metallicity calculated with equation (22), respectively.

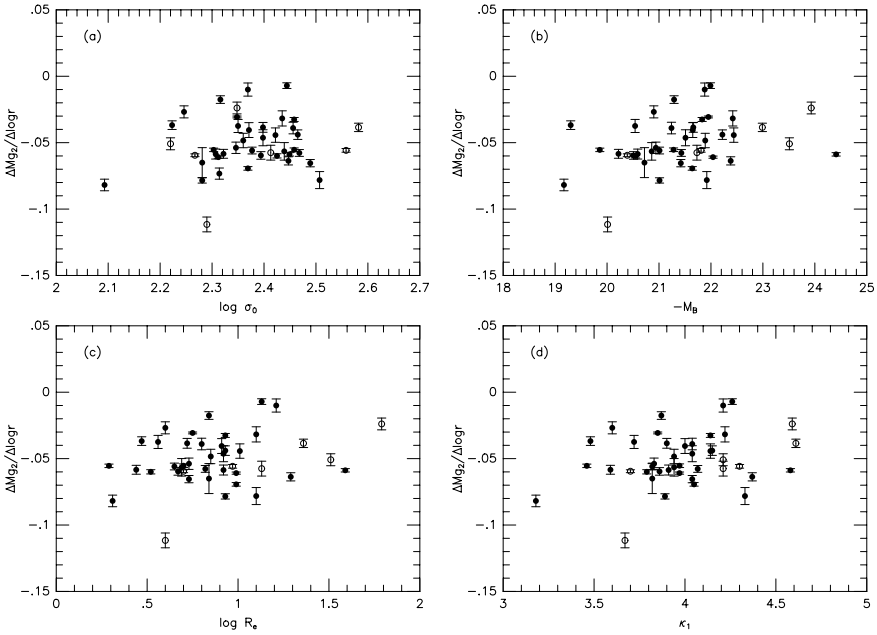

FIG. 6.— The Mg_2 gradient versus the mass tracers; (a) the central velocity dispersion σ_0, (b) the absolute B-magnitude M_B, (c) the absolute effective radius $R_{\rm e}$, and (d) the dynamical mass $\kappa_1 = (\log \sigma_0^2 + \log R_{\rm e})/\sqrt{2}$. Symbols are the same as in figure 5.

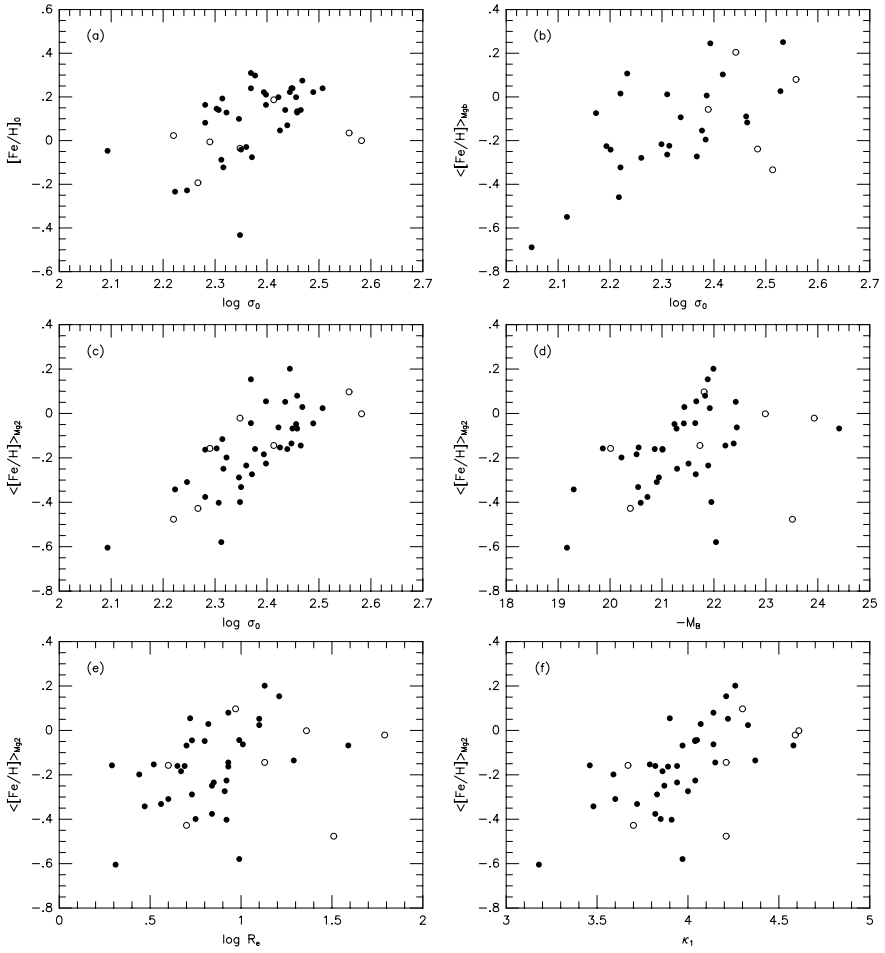

FIG. 7.— The metallicity versus the mass tracers; (a)-(c) σ_0, (d) M_B, (e) R_e, and (f) κ_1. (a) is for the central metallicity derived from the central Mg_2 index, (b) is for the mean stellar metallicity derived from the Mg_b gradient, and (c)-(f) are for the mean stellar metallicity derived from the Mg_2 gradient. Symbols are the same as in figure 5.

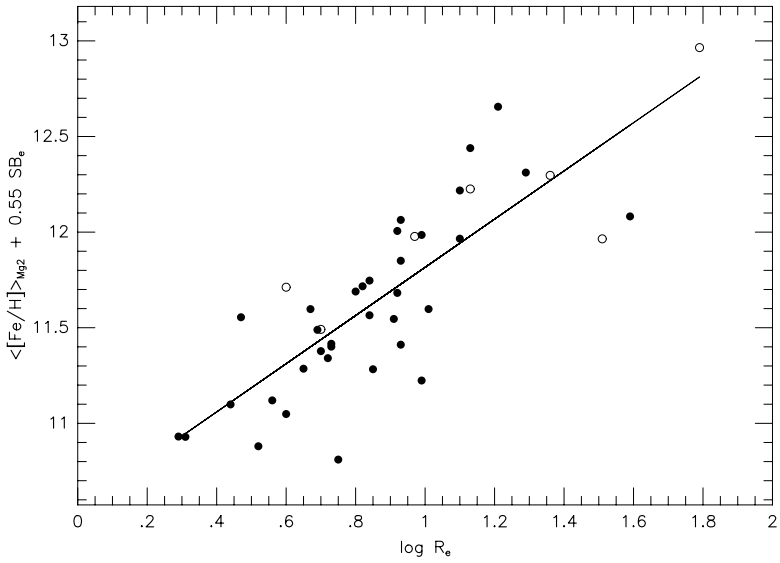

FIG. 8.— The fundamental plane for the absolute radius, the surface brightness, and the mean metallicity. The symbols are the same as in figure 5.

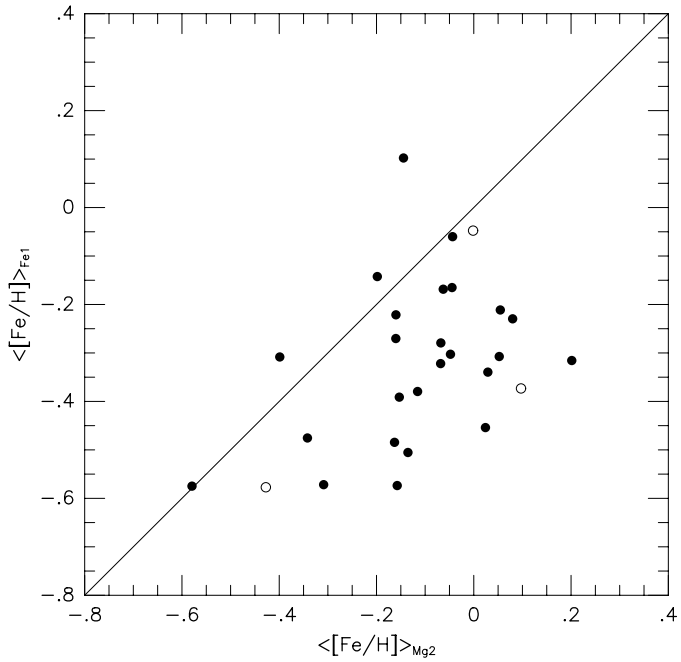

FIG. 9.— Comparison of the mean metallicities derived from Mg_2 and Fe_1. The symbols are the same as in figure 5.

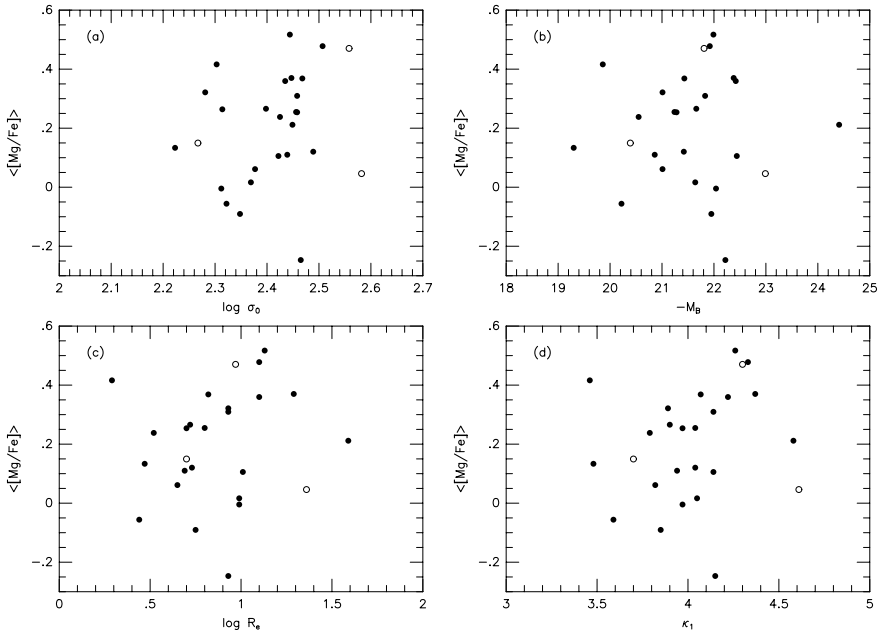

FIG. 10.— The mean [Mg/Fe] ratio versus the mass tracers; (a) σ_0, (b) M_B, (c) $R_{\rm e}$, and (d) κ_1. Symbols are the same as in figure 5.

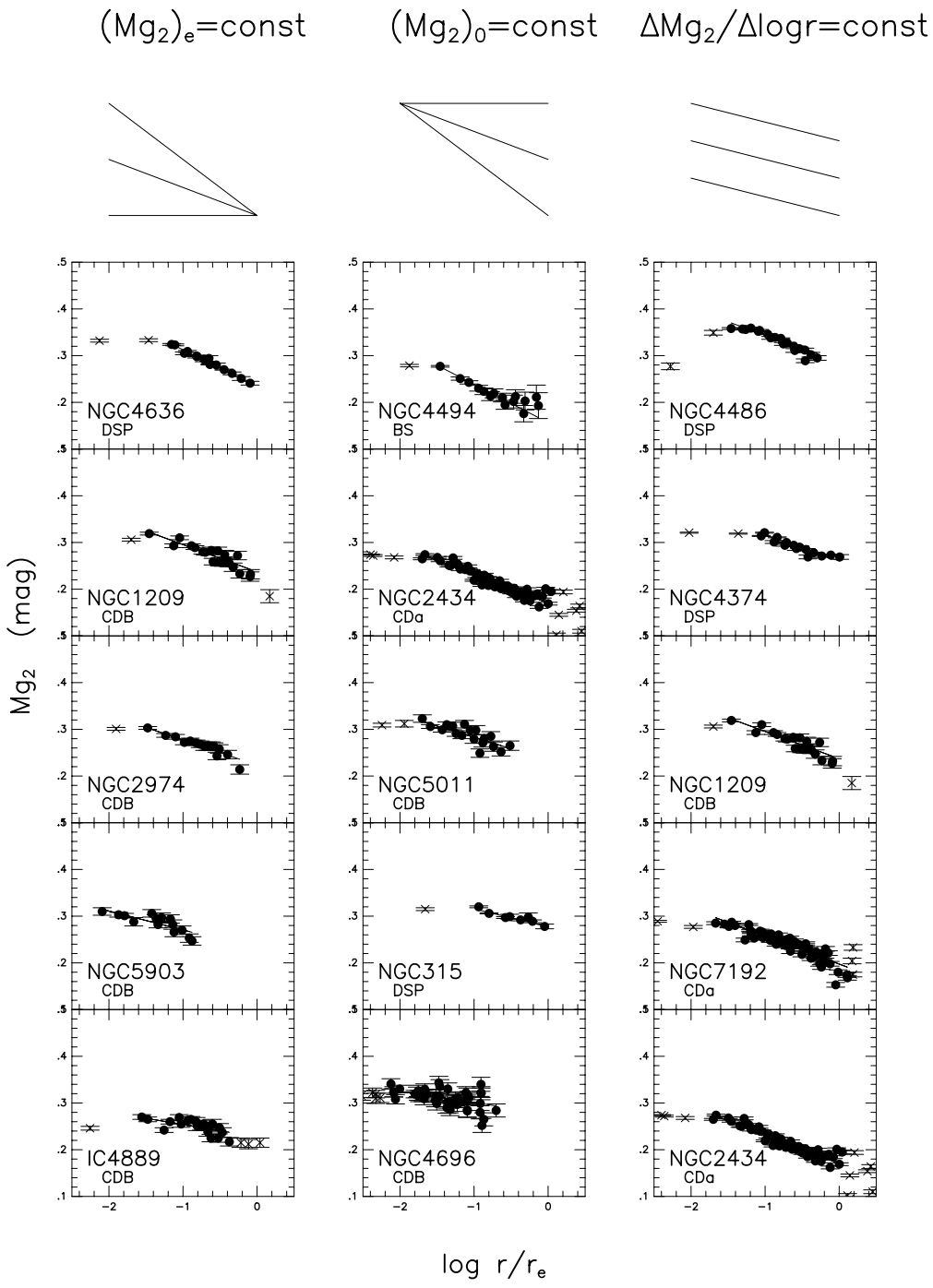

FIG. 11.— The Mg_2 gradients of elliptical galaxies. The left, middle, and right panels give the sequences of $(Mg)_e$ = const., $\log \sigma_0$ = const., and $\Delta Mg_2/\Delta \log r$ = const., respectively.

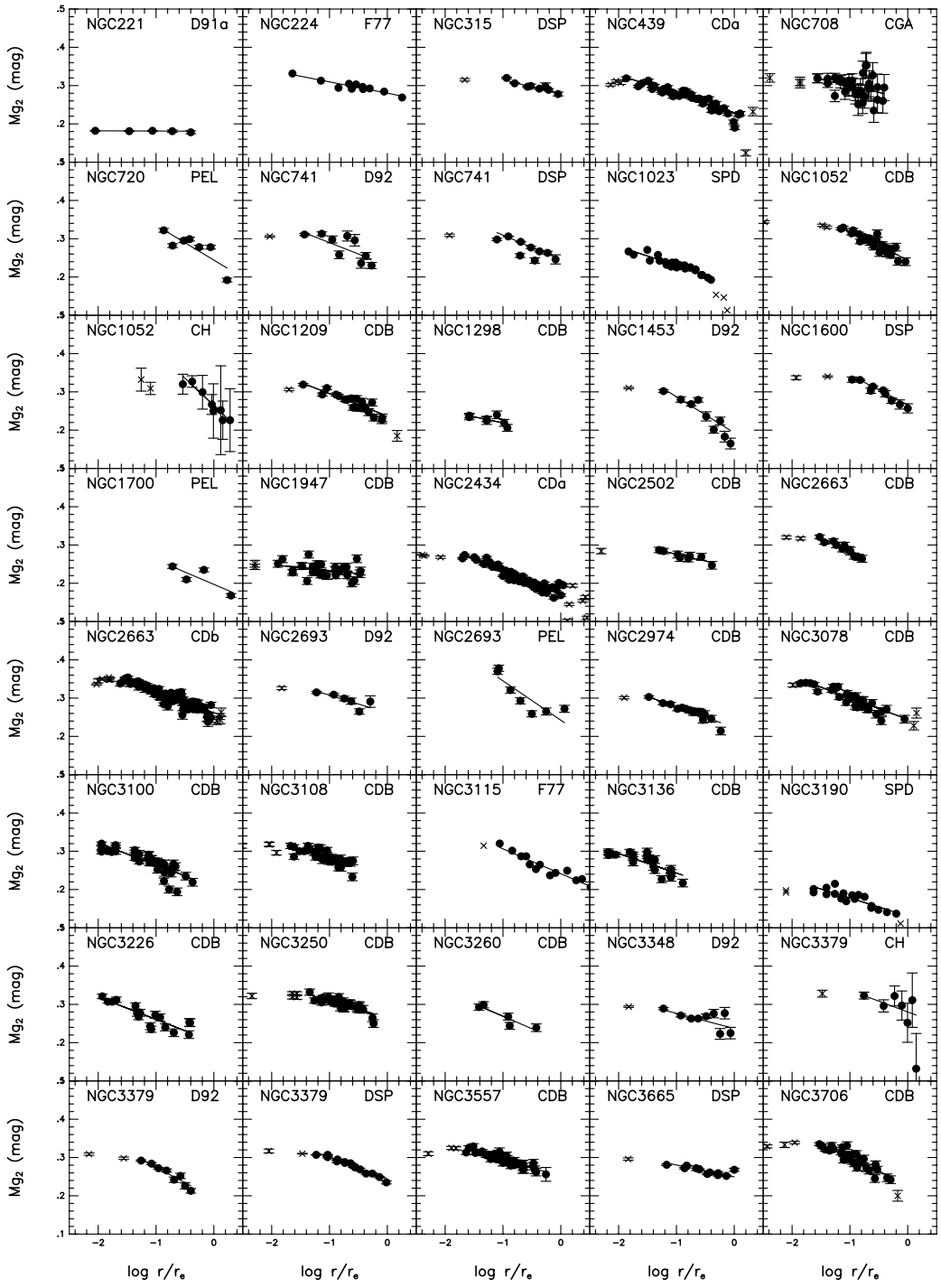

FIG. 12.— The Mg_2 gradients of early-type galaxies.

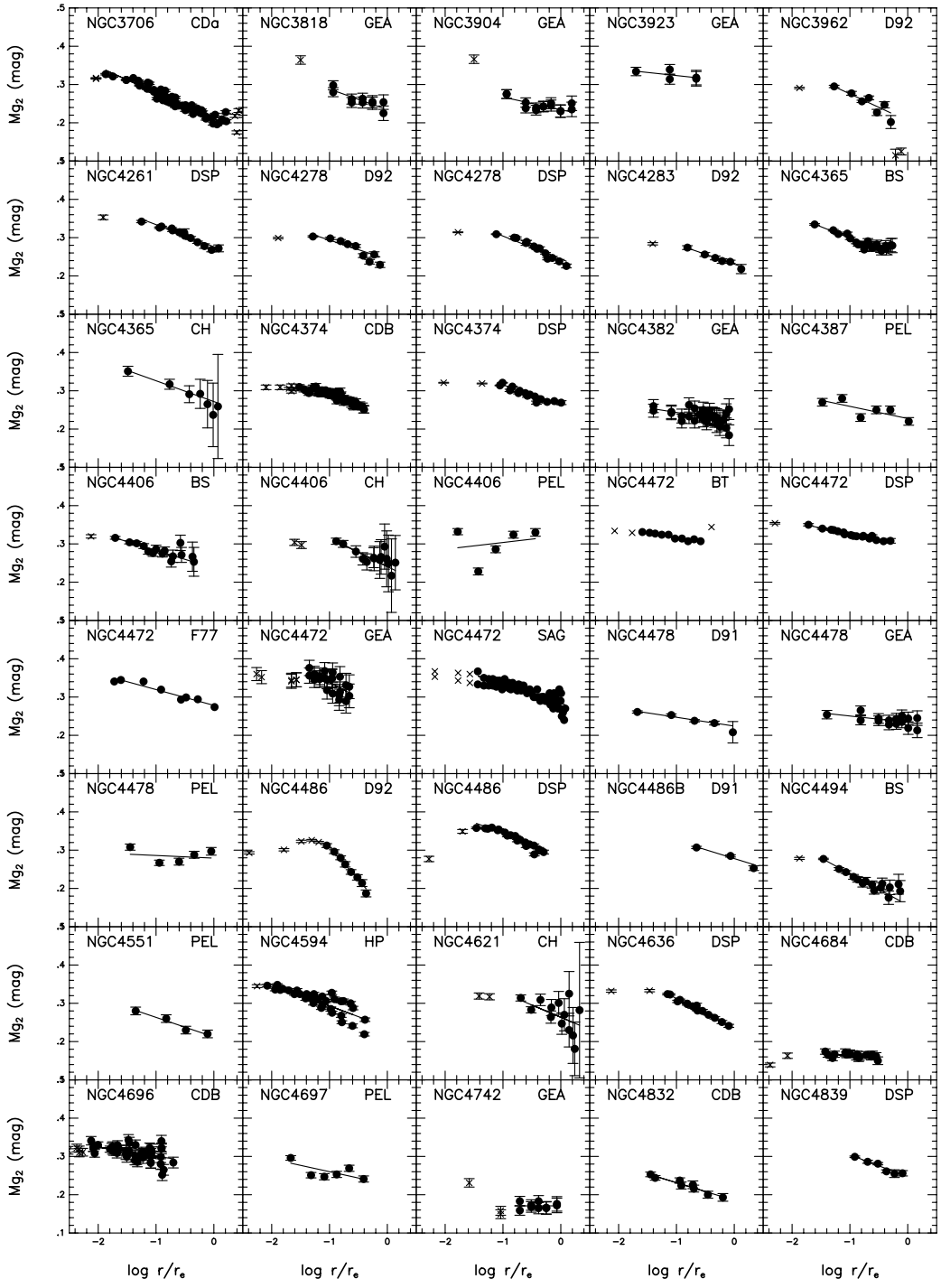
NGC3706 CDa
NGC3818 GEA
NGC3904 GEA
NGC3923 GEA
NGC3962 D92
NGC4261 DSP
NGC4278 D92
NGC4278 DSP
NGC4283 D92
NGC4365 BS
NGC4365 CH
NGC4374 CDB
NGC4374 DSP
NGC4382 GEA
NGC4387 PEL
NGC4406 BS
NGC4406 CH
NGC4406 PEL
NGC4472 BT
NGC4472 DSP
NGC4472 F77
NGC4472 GEA
NGC4472 SAG
NGC4478 D91
NGC4478 GEA
NGC4478 PEL
NGC4486 D92
NGC4486 DSP
NGC4486B D91
NGC4494 BS
NGC4551 PEL
NGC4594 HP
NGC4621 CH
NGC4636 DSP
NGC4684 CDB
NGC4696 CDB
NGC4697 PEL
NGC4742 GEA
NGC4832 CDB
NGC4839 DSP
Mg2 (mag)
log r/re

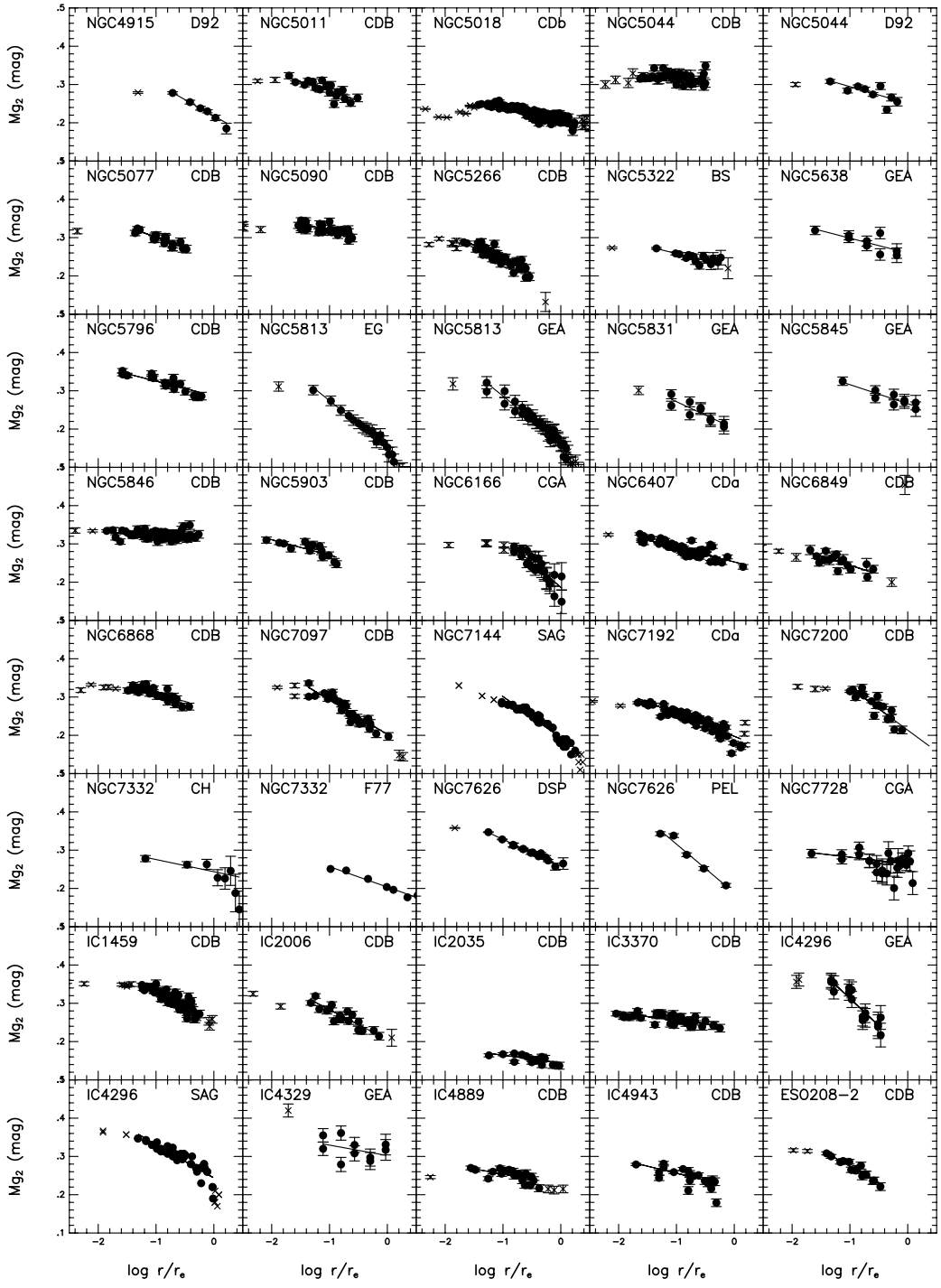
NGC4915 D92
NGC5011 CDB
NGC5018 CDb
NGC5044 CDB
NGC5044 D92
NGC5077 CDB
NGC5090 CDB
NGC5266 CDB
NGC5322 BS
NGC5638 GEA
NGC5796 CDB
NGC5813 EG
NGC5813 GEA
NGC5831 GEA
NGC5845 GEA
NGC5846 CDB
NGC5903 CDB
NGC6166 CGA
NGC6407 CDa
NGC6849 CDB
NGC6868 CDB
NGC7097 CDB
NGC7144 SAG
NGC7192 CDa
NGC7200 CDB
NGC7332 CH
NGC7332 F77
NGC7626 DSP
NGC7626 PEL
NGC7728 CGA
IC1459 CDB
IC2006 CDB
IC2035 CDB
IC3370 CDB
IC4296 GEA
IC4296 SAG
IC4329 GEA
IC4889 CDB
IC4943 CDB
ESO208−2 CDB
Mg2 (mag)
log r/re

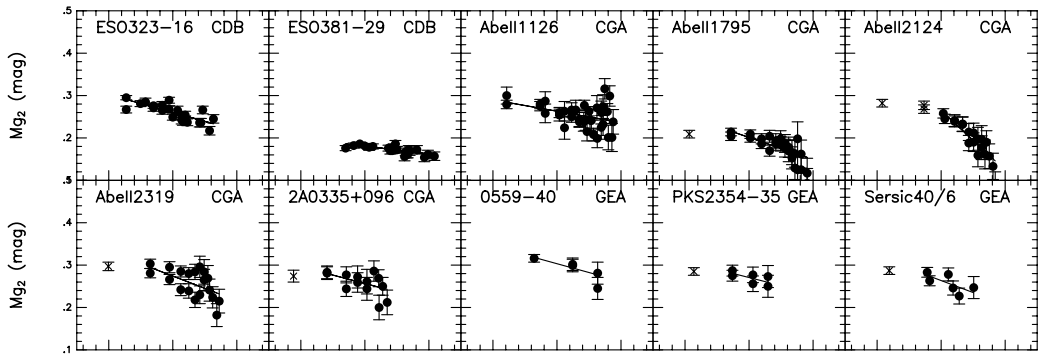
ESO323−16 CDB
ESO381−29 CDB
Abell1126 CGA
Abell1795 CGA
Abell2124 CGA
Abell2319 CGA
2A0335+096 CGA
0559−40 GEA
PKS2354−35 GEA
Sersic40/6 GEA
Mg2 (mag)
Mg2 (mag)

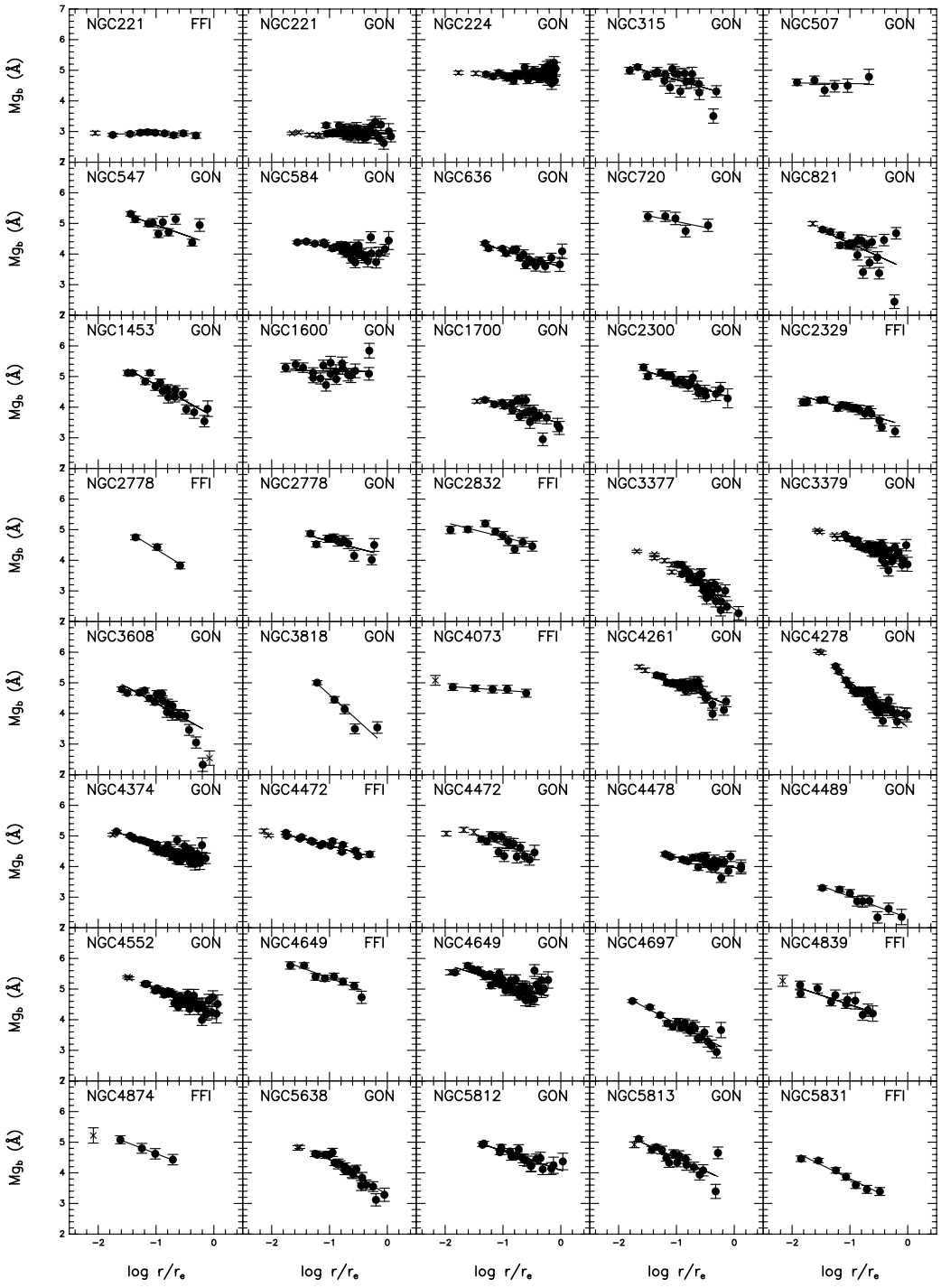

FIG. 13.— The Mg_b gradients of early-type galaxies.

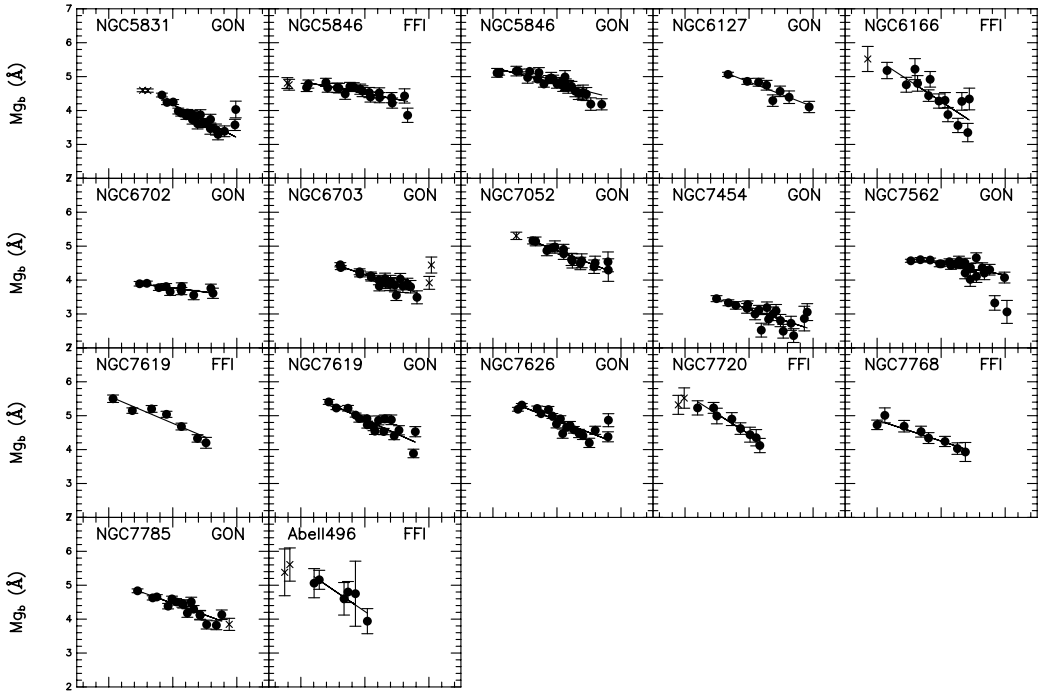
NGC5831 GON
NGC5846 FFI
NGC5846 GON
NGC6127 GON
NGC6166 FFI
NGC6702 GON
NGC6703 GON
NGC7052 GON
NGC7454 GON
NGC7562 GON
NGC7619 FFI
NGC7619 GON
NGC7626 GON
NGC7720 FFI
NGC7768 FFI
NGC7785 GON
Abell496 FFI
Mgb (Å)

TABLE 1
LINE-STRENGTH GRADIENTS OF ELLIPTICAL GALAXIES

Galaxy (1)	Ref. (2)	Index (3)	$(\text{Index})_e$ (4)	Error (5)	$\frac{\Delta\text{Index}}{\Delta \log r}$ (6)	Error (7)
NGC 315	DSP	Mg_2	0.277	0.002	−0.038	0.003
		Fe_1	3.136	0.085	0.142	0.144
		$H\beta$	1.456	0.049	0.131	0.095
NGC 547	GON	Mg_b	4.294	0.109	−0.654	0.099
		Fe_1	2.316	0.127	−0.574	0.117
		Fe_2	2.493	0.173	−0.167	0.160
		$H\beta$	1.363	0.122	0.052	0.111
NGC 584	GON	Mg_b	3.932	0.049	−0.317	0.045
		Fe_1	2.332	0.053	−0.563	0.049
		Fe_2	2.226	0.059	−0.441	0.054
		$H\beta$	2.037	0.045	0.144	0.042
NGC 636	GON	Mg_b	3.585	0.067	−0.546	0.069
		Fe_1	2.698	0.072	−0.411	0.074
		Fe_2	2.267	0.085	−0.483	0.087
		$H\beta$	1.846	0.081	−0.005	0.083
NGC 720	GON	Mg_b	4.673	0.257	−0.388	0.230
		Fe_1	2.553	0.268	−0.318	0.242
		Fe_2	3.082	0.315	0.213	0.284
		$H\beta$	2.478	0.241	0.669	0.218
NGC 741	DSP	Mg_2	0.246	0.002	−0.064	0.003
		Fe_1	2.228	0.159	−0.762	0.173
		$H\beta$	1.698	0.078	0.355	0.098
NGC 821	GON	Mg_b	3.492	0.094	−0.861	0.085
		Fe_1	2.481	0.101	−0.510	0.091
		Fe_2	2.566	0.113	−0.165	0.103
		$H\beta$	2.101	0.086	0.366	0.078
NGC 1052	CDB	Mg_2	0.245	0.004	−0.073	0.004
		Fe_1	2.565	0.194	−0.438	0.230
NGC 1209	CDB	Mg_2	0.237	0.003	−0.058	0.003
		Fe_1	2.920	0.261	−0.426	0.254
NGC 1298	CDB	Mg_2	0.188	0.016	−0.031	0.012
NGC 1453	GON	Mg_b	3.687	0.090	−1.044	0.081
		Fe_1	2.667	0.107	−0.261	0.097
		Fe_2	2.655	0.144	−0.267	0.132
		$H\beta$	1.363	0.101	0.323	0.091
NGC 1600	DSP	Mg_2	0.266	0.004	−0.078	0.006
		Fe_1	2.411	0.078	−0.551	0.127
		$H\beta$	1.832	0.115	0.328	0.140
NGC 1700	GON	Mg_b	3.457	0.079	−0.620	0.083
		Fe_1	2.526	0.085	−0.566	0.090
		Fe_2	2.456	0.099	−0.340	0.105
		$H\beta$	2.090	0.067	0.121	0.071
NGC 2434	CDa	Mg_2	0.171	0.001	−0.061	0.001
		Fe_1	2.294	0.061	−0.376	0.059
		Fe_2	2.101	0.059	−0.306	0.057
NGC 2663	CDb	Mg_2	0.259	0.001	−0.059	0.001
		Fe_1	2.729	0.049	−0.388	0.044
		Fe_2	1.827	0.051	−0.771	0.046
NGC 2778	GON	Mg_b	4.137	0.124	−0.491	0.121
		Fe_1	2.751	0.140	−0.203	0.137
		Fe_2	2.000	0.159	−0.591	0.158
		$H\beta$	0.863	0.143	−0.387	0.151
NGC 2832	FFI	Mg_b	4.285	0.125	−0.475	0.098
		$H\beta$	1.429	0.105	0.018	0.081
NGC 2974	CDB	Mg_2	0.223	0.005	−0.054	0.004
NGC 3078	CDB	Mg_2	0.245	0.003	−0.056	0.003
		Fe_1	2.779	0.261	−0.494	0.189
NGC 3136B	CDB	Mg_2	0.192	0.008	−0.051	0.004
NGC 3226	CDB	Mg_2	0.202	0.005	−0.059	0.004
NGC 3250	CDB	Mg_2	0.265	0.005	−0.044	0.005
		Fe_1	2.768	0.398	−0.691	0.467
NGC 3260	CDB	Mg_2	0.204	0.012	−0.065	0.011
NGC 3377	GON	Mg_b	2.409	0.073	−1.432	0.105
		Fe_1	1.982	0.074	−0.713	0.106
		Fe_2	1.398	0.080	−0.900	0.116
		$H\beta$	1.883	0.065	0.207	0.093
NGC 3379	DSP	Mg_2	0.245	0.001	−0.055	0.001
		Fe_1	2.272	0.025	−0.452	0.032
		Fe_2	2.483	0.074	−0.417	0.100
		$H\beta$	1.636	0.025	0.077	0.025
NGC 3557	CDB	Mg_2	0.251	0.004	−0.044	0.004

TABLE 1—*Continued*

Galaxy (1)	Ref. (2)	Index (3)	$(\text{Index})_e$ (4)	Error (5)	$\frac{\Delta\text{Index}}{\Delta \log r}$ (6)	Error (7)
		Fe_1	3.344	0.445	−0.163	0.398
NGC 3608	GON	Mg_b	3.301	0.085	−1.037	0.073
		Fe_1	3.305	0.094	0.207	0.081
		Fe_2	2.424	0.114	−0.262	0.100
		$H\beta$	1.686	0.111	0.076	0.101
NGC 3818	GON	Mg_b	2.900	0.159	−1.709	0.156
		Fe_1	2.055	0.167	−0.899	0.165
		Fe_2	1.817	0.184	−0.887	0.181
		$H\beta$	1.513	0.143	0.025	0.140
NGC 4073	FFI	Mg_b	4.619	0.163	−0.135	0.121
		$H\beta$	1.095	0.147	−0.291	0.110
NGC 4261	DSP	Mg_2	0.276	0.002	−0.058	0.003
		Fe_1	2.603	0.054	−0.497	0.070
		Fe_2	2.640	0.076	−0.601	0.085
		$H\beta$	1.538	0.019	0.212	0.030
NGC 4278	DSP	Mg_2	0.244	0.001	−0.060	0.002
		Fe_1	2.628	0.016	0.053	0.043
		Fe_2	2.294	0.014	−0.388	0.031
		$H\beta$	1.372	0.029	1.289	0.049
NGC 4365	BS	Mg_2	0.239	0.003	−0.060	0.003
NGC 4374	DSP	Mg_2	0.260	0.001	−0.055	0.001
		Fe_1	2.717	0.048	−0.150	0.061
		Fe_2	2.350	0.075	−0.410	0.095
		$H\beta$	1.697	0.042	0.326	0.052
NGC 4406	BS	Mg_2	0.237	0.008	−0.046	0.006
NGC 4472	DSP	Mg_2	0.292	0.002	−0.033	0.001
		Fe_1	2.803	0.043	−0.388	0.040
		Fe_2	2.754	0.054	−0.594	0.053
		$H\beta$	1.347	0.028	−0.061	0.026
NGC 4478	GON	Mg_b	3.972	0.055	−0.326	0.069
		Fe_1	2.355	0.061	−0.605	0.077
		Fe_2	2.244	0.072	−0.490	0.090
		$H\beta$	1.685	0.072	−0.148	0.093
NGC 4486	DSP	Mg_2	0.289	0.001	−0.056	0.001
		Fe_1	2.587	0.034	−0.398	0.038
		Fe_2	2.763	0.075	−0.306	0.076
		$H\beta$	1.377	0.043	0.535	0.050
NGC 4489	GON	Mg_b	2.328	0.123	−0.695	0.105
		Fe_1	2.415	0.124	−0.414	0.106
		Fe_2	1.711	0.131	−0.575	0.112
		$H\beta$	2.269	0.109	−0.036	0.094
NGC 4494	BS	Mg_2	0.157	0.006	−0.082	0.004
NGC 4552	GON	Mg_b	4.248	0.048	−0.756	0.056
		Fe_1	2.522	0.053	−0.445	0.062
		Fe_2	2.391	0.060	−0.465	0.072
		$H\beta$	1.646	0.040	0.318	0.046
NGC 4636	DSP	Mg_2	0.234	0.001	−0.078	0.002
		Fe_1	2.367	0.057	−0.549	0.070
		Fe_2	2.727	0.090	−0.294	0.104
		$H\beta$	1.995	0.082	0.676	0.096
NGC 4649	GON	Mg_b	4.636	0.051	−0.584	0.042
		Fe_1	2.341	0.056	−0.523	0.046
		Fe_2	2.337	0.073	−0.539	0.062
		$H\beta$	1.255	0.042	−0.056	0.034
NGC 4696	CDB	Mg_2	0.277	0.007	−0.024	0.004
NGC 4697	GON	Mg_b	2.896	0.072	−0.979	0.055
		Fe_1	2.000	0.079	−0.747	0.060
		Fe_2	1.688	0.089	−0.746	0.068
		$H\beta$	1.732	0.064	0.070	0.050
NGC 4839	DSP	Mg_2	0.247	0.004	−0.058	0.006
		$H\beta$	1.252	0.118	−0.098	0.175
NGC 4874	FFI	Mg_b	3.902	0.284	−0.725	0.224
		$H\beta$	1.383	0.260	−0.027	0.201
NGC 5011	CDB	Mg_2	0.234	0.007	−0.048	0.005
NGC 5018	CDb	Mg_2	0.211	0.001	−0.031	0.001
		Fe_1	2.702	0.028	−0.332	0.029
		Fe_2	2.470	0.029	−0.463	0.031
NGC 5044	CDB	Mg_2	0.309	0.005	−0.010	0.005
NGC 5077	CDB	Mg_2	0.244	0.007	−0.057	0.007
		Fe_1	2.750	0.384	−0.362	0.376
NGC 5090	CDB	Mg_2	0.288	0.006	−0.032	0.006

TABLE 1—*Continued*

Galaxy (1)	Ref. (2)	Index (3)	$(\mathrm{Index})_e$ (4)	Error (5)	$\frac{\Delta \mathrm{Index}}{\Delta \log r}$ (6)	Error (7)
		Fe_1	2.692	0.504	−0.373	0.448
NGC 5322	BS	Mg_2	0.221	0.005	−0.037	0.005
NGC 5638	GON	Mg_b	3.286	0.079	−1.152	0.085
		Fe_1	2.521	0.083	−0.384	0.091
		Fe_2	2.162	0.092	−0.429	0.101
		$H\beta$	1.694	0.082	0.037	0.089
NGC 5796	CDB	Mg_2	0.287	0.004	−0.038	0.004
		Fe_1	2.795	0.308	−0.491	0.255
NGC 5812	GON	Mg_b	4.091	0.076	−0.622	0.074
		Fe_1	2.604	0.081	−0.446	0.080
		Fe_2	2.460	0.090	−0.498	0.089
		$H\beta$	1.679	0.068	−0.036	0.067
NGC 5813	GON	Mg_b	3.637	0.105	−0.847	0.085
		Fe_1	2.844	0.118	−0.059	0.097
		Fe_2	2.320	0.151	−0.146	0.124
		$H\beta$	0.945	0.129	−0.188	0.104
NGC 5831	GON	Mg_b	3.203	0.067	−0.973	0.077
		Fe_1	2.516	0.072	−0.497	0.083
		Fe_2	2.106	0.080	−0.657	0.093
		$H\beta$	1.988	0.070	0.106	0.079
NGC 5846	CDB	Mg_2	0.317	0.003	−0.007	0.002
		Fe_1	2.683	0.161	−0.360	0.127
NGC 5903	CDB	Mg_2	0.230	0.009	−0.041	0.006
NGC 6127	GON	Mg_b	4.113	0.109	−0.728	0.105
		Fe_1	2.304	0.121	−0.503	0.118
		Fe_2	2.482	0.140	−0.200	0.138
		$H\beta$	1.522	0.096	0.030	0.092
NGC 6166	FFI	Mg_b	3.029	0.210	−1.236	0.182
		$H\beta$	2.388	0.172	1.293	0.141
NGC 6702	GON	Mg_b	3.530	0.101	−0.236	0.085
		Fe_1	2.649	0.117	−0.306	0.099
		Fe_2	2.627	0.147	−0.258	0.123
		$H\beta$	2.155	0.119	0.001	0.100
NGC 6868	CDB	Mg_2	0.269	0.005	−0.039	0.004
		Fe_1	2.604	0.229	−0.621	0.211
NGC 7052	GON	Mg_b	4.137	0.127	−0.734	0.122
		Fe_1	2.543	0.139	−0.278	0.134
		Fe_2	2.555	0.163	−0.178	0.160
		$H\beta$	2.316	0.118	0.962	0.113
NGC 7097	CDB	Mg_2	0.203	0.003	−0.090	0.004
		Fe_1	1.972	0.232	−0.990	0.250
NGC 7192	CDa	Mg_2	0.197	0.001	−0.059	0.001
		Fe_1	2.256	0.040	−0.481	0.039
		Fe_2	1.786	0.042	−0.647	0.041
NGC 7200	CDB	Mg_2	0.213	0.004	−0.112	0.006
NGC 7454	GON	Mg_b	2.533	0.095	−0.610	0.090
		Fe_1	2.076	0.096	−0.462	0.092
		Fe_2	1.973	0.104	−0.266	0.099
		$H\beta$	1.962	0.085	−0.100	0.081
NGC 7562	GON	Mg_b	4.151	0.059	−0.331	0.054
		Fe_1	2.944	0.063	−0.082	0.059
		Fe_2	2.194	0.072	−0.391	0.067
		$H\beta$	1.590	0.057	−0.029	0.052
NGC 7619	GON	Mg_b	4.040	0.066	−0.846	0.059
		Fe_1	2.245	0.077	−0.650	0.069
		Fe_2	2.541	0.109	−0.433	0.099
		$H\beta$	1.549	0.073	0.119	0.063
NGC 7626	DSP	Mg_2	0.259	0.001	−0.069	0.001
		Fe_1	3.118	0.039	0.005	0.040
		Fe_2	2.674	0.050	−0.448	0.062
		$H\beta$	1.256	0.032	−0.050	0.028
NGC 7720	FFI	Mg_b	3.272	0.294	−1.186	0.225
		$H\beta$	2.616	0.261	0.947	0.199
NGC 7768	FFI	Mg_b	3.630	0.187	−0.620	0.133
		$H\beta$	1.319	0.197	−0.030	0.140
NGC 7785	GON	Mg_b	3.785	0.070	−0.679	0.063
		Fe_1	2.625	0.082	−0.247	0.075
		Fe_2	2.648	0.105	−0.219	0.096
		$H\beta$	1.568	0.084	0.048	0.076
IC 1459	CDB	Mg_2	0.260	0.003	−0.065	0.003
		Fe_1	2.885	0.195	−0.431	0.200

TABLE 1—*Continued*

Galaxy (1)	Ref. (2)	Index (3)	$(\text{Index})_e$ (4)	Error (5)	$\frac{\Delta\text{Index}}{\Delta \log r}$ (6)	Error (7)
IC 3370	CDB	Mg_2	0.239	0.004	−0.018	0.003
IC 4889	CDB	Mg_2	0.227	0.005	−0.027	0.005
IC 4943	CDB	Mg_2	0.219	0.004	−0.037	0.003
		Fe_1	2.359	0.217	−0.598	0.198
Abell 496	FFI	Mg_b	2.936	0.750	−1.291	0.516
ESO 323-16	CDB	Mg_2	0.218	0.005	−0.042	0.004

Col.(1).—Galaxy ID.

Col.(2).—Reference.

Col.(3).—Index.

Col.(4)(5).—Intercept at the effective radius and the error.

Col.(6)(7).—Gradient and the error.

TABLE 2
METALLICITY GRADIENTS AND MEAN METALLICITIES OF ELLIPTICAL GALAXIES

		Mg_2		Mg_b		Fe_1		Fe_2		Mg_2	Mg_b	Fe_1	Fe_2
Galaxy	Ref.	Z_e	c	Z_e	c	Z_e	c	Z_e	c		$\langle$[Fe/H]$\rangle$		
(1)	(2)	(3)	(4)	(5)	(6)	(7)	(8)	(9)	(10)	(11)	(12)	(13)	(14)
NGC 315	DSP	0.0185	−0.225			0.0179	0.096			0.00		−0.05	
NGC 547	GON			0.0227	−0.293	0.0050	−0.387	0.0099	−0.098		0.11	−0.51	−0.30
NGC 584	GON			0.0156	−0.142	0.0051	−0.380	0.0069	−0.260		−0.09	−0.50	−0.42
NGC 636	GON			0.0109	−0.245	0.0091	−0.277	0.0073	−0.285		−0.23	−0.30	−0.39
NGC 720	GON			0.0335	−0.174	0.0072	−0.214	0.0220	0.126		0.25	−0.41	0.04
NGC 741	DSP	0.0121	−0.372			0.0044	−0.514			−0.14		−0.51	
NGC 821	GON			0.0099	−0.386	0.0065	−0.344	0.0109	−0.097		−0.22	−0.42	−0.25
NGC 1052	CDB	0.0119	−0.428			0.0074	−0.295			−0.12		−0.38	
NGC 1209	CDB	0.0108	−0.341			0.0128	−0.287			−0.20		−0.14	
NGC 1298	CDB	0.0056	−0.183							−0.53			
NGC 1453	GON			0.0121	−0.468	0.0086	−0.176	0.0123	−0.157		−0.09	−0.34	−0.19
NGC 1600	DSP	0.0159	−0.457			0.0058	−0.372			0.02		−0.45	
NGC 1700	GON			0.0096	−0.278	0.0069	−0.382	0.0094	−0.200		−0.27	−0.37	−0.30
NGC 2434	CDa	0.0044	−0.356			0.0048	−0.253	0.0058	−0.180	−0.58		−0.57	−0.51
NGC 2663	CDb	0.0145	−0.344			0.0095	−0.262	0.0040	−0.454	−0.07		−0.28	−0.58
NGC 2778	GON			0.0193	−0.220	0.0099	−0.137	0.0051	−0.349		0.02	−0.29	−0.52
NGC 2832	FFI			0.0224	−0.213						0.08		
NGC 2974	CDB	0.0090	−0.315							−0.29			
NGC 3078	CDB	0.0119	−0.327			0.0103	−0.333			−0.16		−0.22	
NGC 3136B	CDB	0.0059	−0.297							−0.48			
NGC 3226	CDB	0.0067	−0.342							−0.40			
NGC 3250	CDB	0.0157	−0.259			0.0101	−0.466			−0.06		−0.17	
NGC 3260	CDB	0.0069	−0.380							−0.38			
NGC 3377	GON			0.0032	−0.642	0.0030	−0.481	0.0022	−0.530		−0.55	−0.69	−0.79
NGC 3379	DSP	0.0120	−0.324			0.0047	−0.305	0.0098	−0.246	−0.16		−0.57	−0.27
NGC 3557	CDB	0.0130	−0.257			0.0247	−0.110			−0.14		0.10	
NGC 3608	GON			0.0081	−0.465	0.0233	0.140	0.0090	−0.155		−0.26	0.07	−0.33
NGC 3818	GON			0.0054	−0.766	0.0033	−0.606	0.0040	−0.523		−0.22	−0.56	−0.54
NGC 4073	FFI			0.0317	−0.061						0.20		
NGC 4261	DSP	0.0182	−0.338			0.0078	−0.335	0.0121	−0.354	0.03		−0.34	−0.14
NGC 4278	DSP	0.0119	−0.350			0.0081	0.036	0.0076	−0.229	−0.15		−0.39	−0.39
NGC 4365	BS	0.0111	−0.348							−0.18			
NGC 4374	DSP	0.0148	−0.323			0.0093	−0.101	0.0082	−0.242	−0.07		−0.32	−0.35
NGC 4406	BS	0.0107	−0.271							−0.23			
NGC 4472	DSP	0.0227	−0.190			0.0107	−0.262	0.0141	−0.350	0.08		−0.23	−0.08
NGC 4478	GON			0.0163	−0.146	0.0053	−0.408	0.0071	−0.289		−0.07	−0.48	−0.40
NGC 4486	DSP	0.0216	−0.326			0.0076	−0.269	0.0143	−0.180	0.10		−0.37	−0.12
NGC 4489	GON			0.0030	−0.312	0.0058	−0.279	0.0034	−0.339		−0.77	−0.49	−0.70
NGC 4494	BS	0.0037	−0.478							−0.60			
NGC 4552	GON			0.0216	−0.339	0.0069	−0.300	0.0086	−0.274		0.10	−0.41	−0.32
NGC 4636	DSP	0.0103	−0.458			0.0054	−0.371	0.0136	−0.173	−0.16		−0.48	−0.15
NGC 4649	GON			0.0323	−0.262	0.0052	−0.353	0.0080	−0.318		0.25	−0.51	−0.34
NGC 4696	CDB	0.0184	−0.140							−0.02			
NGC 4697	GON			0.0054	−0.439	0.0031	−0.503	0.0033	−0.440		−0.46	−0.67	−0.67
NGC 4839	DSP	0.0123	−0.336							−0.14			
NGC 4874	FFI			0.0151	−0.325						−0.06		
NGC 5011	CDB	0.0104	−0.283							−0.23			
NGC 5018	CDb	0.0076	−0.179			0.0091	−0.224	0.0096	−0.273	−0.40		−0.31	−0.27
NGC 5044	CDB	0.0283	−0.059							0.15			
NGC 5077	CDB	0.0119	−0.331			0.0098	−0.244			−0.16		−0.27	
NGC 5090	CDB	0.0214	−0.186			0.0090	−0.252			0.05		−0.31	
NGC 5322	BS	0.0087	−0.219							−0.33			
NGC 5638	GON			0.0080	−0.517	0.0069	−0.259	0.0063	−0.253		−0.24	−0.42	−0.46
NGC 5796	CDB	0.0210	−0.225			0.0105	−0.331			0.05		−0.21	
NGC 5812	GON			0.0184	−0.279	0.0078	−0.301	0.0095	−0.294		0.01	−0.35	−0.27
NGC 5813	GON			0.0115	−0.380	0.0114	−0.040	0.0078	−0.086		−0.15	−0.24	−0.40
NGC 5831	GON			0.0073	−0.436	0.0068	−0.335	0.0059	−0.387		−0.32	−0.40	−0.44
NGC 5846	CDB	0.0316	−0.041			0.0089	−0.243			0.20		−0.32	
NGC 5903	CDB	0.0098	−0.237							−0.27			
NGC 6127	GON			0.0188	−0.327	0.0049	−0.339	0.0098	−0.118		0.04	−0.54	−0.30
NGC 6166	FFI			0.0061	−0.554						−0.33		
NGC 6702	GON			0.0103	−0.106	0.0084	−0.206	0.0119	−0.152		−0.28	−0.35	−0.21
NGC 6868	CDB	0.0166	−0.228			0.0078	−0.419			−0.05		−0.30	
NGC 7052	GON			0.0193	−0.329	0.0071	−0.187	0.0108	−0.105		0.05	−0.42	−0.26
NGC 7097	CDB	0.0068	−0.526			0.0029	−0.668			−0.31		−0.57	
NGC 7192	CDa	0.0063	−0.348			0.0046	−0.325	0.0038	−0.382	−0.43		−0.58	−0.64
NGC 7200	CDB	0.0078	−0.652							−0.16			
NGC 7454	GON			0.0037	−0.273	0.0035	−0.312	0.0049	−0.157		−0.69	−0.70	−0.59
NGC 7562	GON			0.0196	−0.148	0.0133	−0.056	0.0066	−0.231		0.01	−0.17	−0.45
NGC 7619	GON			0.0174	−0.379	0.0045	−0.438	0.0106	−0.255		0.03	−0.54	−0.24
NGC 7626	DSP	0.0145	−0.405			0.0174	0.004	0.0127	−0.264	−0.04		−0.06	−0.15

TABLE 2—*Continued*

Galaxy	Ref.	Mg_2		Mg_b		Fe_1		Fe_2		Mg_2	Mg_b	Fe_1	Fe_2
		Z_e	c	Z_e	c	Z_e	c	Z_e	c		$\langle$[Fe/H]$\rangle$		
(1)	(2)	(3)	(4)	(5)	(6)	(7)	(8)	(9)	(10)	(11)	(12)	(13)	(14)
NGC 7720	FFI			0.0079	−0.532						−0.24		
NGC 7768	FFI			0.0114	−0.278						−0.20		
NGC 7785	GON			0.0134	−0.305	0.0081	−0.166	0.0122	−0.129		−0.12	−0.37	−0.20
IC 1459	CDB	0.0148	−0.382			0.0121	−0.290			−0.04		−0.17	
IC 3370	CDB	0.0110	−0.103							−0.25			
IC 4889	CDB	0.0094	−0.157							−0.31			
IC 4943	CDB	0.0085	−0.215			0.0054	−0.403			−0.34		−0.48	
Abell 496	FFI			0.0056	−0.579						−0.36		
ESO 323-16	CDB	0.0084	−0.246							−0.34			

Col.(1).—Galaxy ID.

Col.(2).—Reference.

Col.(3)(5)(7)(9).—Gradients for Mg_2, Fe_1, Fe_2, and Mg_b.

Col.(4)(6)(8)(10).—Intercepts at the effective radius for Mg_2, Fe_1, Fe_2, and Mg_b.

Col.(11)(12)(13)(14).—Mean metallicities for Mg_2, Fe_1, Fe_2, and Mg_b.

TABLE 3A
MEAN METALLICITIES CORRECTED WITH $H\beta$

Galaxy	Ref.	eq.(22)(2)(4)	eq.(22)(5)(10)		eq.(22)(6)(8)		
		$\langle$[Fe/H]$\rangle$	$(t_9)_e$	$\langle$[Fe/H]$\rangle$	$(t_9)_e$	Δt_9	$\langle$[Fe/H]$\rangle$
(1)	(2)	(3)	(4)	(5)	(6)	(7)	(8)
NGC 315	DSP	0.00	15.6	0.02	15.4	−0.1	0.03
NGC 741	DSP	−0.14	9.9	0.01	10.6	−5.0	−0.03
NGC 1600	DSP	0.02	6.7	0.21	3.6	−2.3	0.27
NGC 3379	DSP	−0.16	11.4	−0.04	12.8	3.7	−0.05
NGC 4261	DSP	0.03	13.7	0.08	12.7	−0.7	0.10
NGC 4278	DSP	−0.15	17.6	−0.18	22.2	−38.0	−0.15
NGC 4374	DSP	−0.07	9.9	0.08	8.9	−4.9	0.08
NGC 4472	DSP	0.08	18.2	0.04	17.4	5.9	0.08
NGC 4486	DSP	0.10	17.5	0.06	16.8	−12.2	0.04
NGC 4636	DSP	−0.16	2.9	0.12	1.6	−14.5	0.09
NGC 4839	DSP	−0.14	20.4	−0.24	26.1	10.1	−0.29
NGC 7626	DSP	−0.04	20.3	−0.15	24.5	9.8	−0.16

Col.(1).—Galaxy ID.

Col.(2).—Reference.

Col.(3)(5)(8).—Mean metallicities calculated with (4),(10), and (8), respectively.

Col.(4)(6).—Age at the effective radius

Col.(7).—Age gradient

TABLE 3B
MEAN METALLICITIES CORRECTED WITH $H\beta$

Galaxy (1)	Ref. (2)	eq.(22)(2)(4) $\langle$[Fe/H]$\rangle$ (3)	eq.(22)(5)(10) t_9 (4)	$\langle$[Fe/H]$\rangle$ (5)	eq.(22)(6)(8) $(t_9)_e$ (6)	Δt_9 (7)	$\langle$[Fe/H]$\rangle$ (8)
NGC 547	GON	0.11	17.8	0.06	17.1	4.5	0.11
NGC 584	GON	−0.09	1.9	0.28	−4.4	−2.2	0.44
NGC 636	GON	−0.23	6.4	0.03	6.2	5.6	0.07
NGC 720	GON	0.25	−8.5	0.88	−28.1	−21.0	1.45
NGC 821	GON	−0.22	0.4	0.17	−2.4	−5.1	0.22
NGC 1453	GON	−0.09	17.8	−0.16	23.1	−1.7	−0.31
NGC 1700	GON	−0.27	0.7	0.13	−1.7	1.6	0.19
NGC 2778	GON	0.02	29.6	−0.32	37.2	19.2	−0.35
NGC 2832	FFI	0.08	16.2	0.08	14.7	4.0	0.14
NGC 3377	GON	−0.55	5.5	−0.34	16.4	6.5	−0.53
NGC 3608	GON	−0.26	10.2	−0.14	14.9	7.4	−0.18
NGC 3818	GON	−0.22	14.3	−0.29	25.3	16.0	−0.29
NGC 4073	FFI	0.20	24.1	0.01	23.8	12.1	0.07
NGC 4478	GON	−0.07	10.2	0.09	8.3	8.7	0.18
NGC 4489	GON	−0.77	−3.5	−0.26	2.9	8.2	−0.36
NGC 4552	GON	0.10	11.1	0.22	7.0	−4.3	0.30
NGC 4649	GON	0.25	20.3	0.14	17.7	7.9	0.26
NGC 4697	GON	−0.46	9.1	−0.30	17.2	7.1	−0.43
NGC 4874	FFI	−0.06	17.3	−0.09	20.2	8.2	−0.10
NGC 5638	GON	−0.24	10.0	−0.12	14.7	10.0	−0.12
NGC 5812	GON	0.01	10.4	0.16	7.3	7.5	0.29
NGC 5813	GON	−0.15	27.6	−0.46	39.1	15.4	−0.59
NGC 5831	GON	−0.32	3.1	−0.01	4.7	5.7	0.01
NGC 6127	GON	0.04	14.0	0.08	12.9	6.1	0.16
NGC 6166	FFI	−0.33	−6.4	0.20	−8.5	−35.8	0.23
NGC 6702	GON	−0.28	−0.8	0.18	−4.8	2.3	0.28
NGC 7052	GON	0.05	−4.7	0.57	−16.8	−28.4	0.95
NGC 7454	GON	−0.69	3.7	−0.36	12.2	9.7	−0.50
NGC 7562	GON	0.01	12.5	0.11	10.1	4.3	0.19
NGC 7619	GON	0.03	13.4	0.08	12.7	4.0	0.13
NGC 7720	FFI	−0.24	−11.7	0.43	−19.4	−23.4	0.54
NGC 7768	FFI	−0.20	18.8	−0.26	25.2	7.2	−0.38
NGC 7785	GON	−0.12	13.0	−0.04	14.5	4.9	−0.04

Col.(1).—Galaxy ID.

Col.(2).—Reference.

Col.(3)(5)(8).—Mean metallicities calculated with (4),(10), and (8), respectively.

Col.(4)(6).—Age at the effective radius

Col.(7).—Age gradient

TABLE 4
PHYSICAL PROPERTIES OF ELLIPTICAL GALAXIES

Galaxy	Ref.	Type	$(Mg_2)_0$ [mag]	$\log \sigma_0$ [km s^{-1}]	$\log R_e$ [kpc]	M_B [mag]	κ_1
(1)	(2)	(3)	(4)	(5)	(6)	(7)	(8)
NGC 315	DSP	cD	0.283	2.582	1.36	−22.99	4.61
NGC 547	GON	E	0.319	2.233			
NGC 584	GON	E	0.283	2.336	0.46	−20.41	3.63
NGC 636	GON	E	0.273	2.193	0.29	−19.31	3.31
NGC 720	GON	E	0.330	2.393	0.70	−20.92	3.88
NGC 741	DSP	E	0.324	2.447	1.29	−22.38	4.37
NGC 821	GON	E	0.304	2.299	0.87	−21.08	3.87
NGC 1052	CDB	E	0.316	2.314			
NGC 1209	CDB	E	0.305	2.322	0.44	−20.22	3.59
NGC 1298	CDB	cD					
NGC 1453	GON	E	0.327	2.462	0.98	−21.98	4.17
NGC 1600	DSP	E	0.324	2.507	1.10	−21.92	4.33
NGC 1700	GON	E	0.278	2.367	0.47	−20.99	3.68
NGC 2434	CDa	E	0.268	2.312	0.99	−22.04	3.97
NGC 2663	CDb	E	0.324	2.449	1.59	−24.41	4.58
NGC 2778	GON	E	0.313	2.220	0.58	−20.07	3.55
NGC 2832	FFI	cD	0.340	2.558		−22.20	
NGC 2974	CDB	E	0.300	2.346	0.73	−20.94	3.83
NGC 3078	CDB	E	0.334	2.377	0.65	−21.01	3.82
NGC 3136B	CDB	cD	0.287	2.220	1.51	−23.51	4.21
NGC 3226	CDB	E	0.307	2.307	0.92	−20.59	3.91
NGC 3250	CDB	E	0.317	2.422	1.01	−22.44	4.14
NGC 3260	CDB	E	0.297	2.281	0.84	−20.72	3.82
NGC 3377	GON	E	0.270	2.117	0.28	−19.19	3.19
NGC 3379	DSP	E	0.308	2.303	0.29	−19.86	3.46
NGC 3557	CDB	E	0.307	2.465	0.93	−22.22	4.15
NGC 3608	GON	E	0.312	2.310	0.64	−20.34	3.72
NGC 3818	GON	E	0.315	2.314	0.67	−20.75	3.75
NGC 4073	FFI	cD	0.321	2.442	1.35	−22.39	4.41
NGC 4261	DSP	E	0.330	2.468	0.82	−21.43	4.07
NGC 4278	DSP	E	0.291	2.425	0.52	−20.55	3.79
NGC 4365	BS	E	0.321	2.394	0.67	−20.51	3.86
NGC 4374	DSP	E	0.305	2.458	0.70	−21.28	3.97
NGC 4406	BS	E	0.311	2.398	0.92	−21.51	4.04
NGC 4472	DSP	E	0.306	2.458	0.93	−21.83	4.14
NGC 4478	GON	E	0.253	2.173	0.10	−19.19	3.14
NGC 4486	DSP	cD	0.289	2.558	0.97	−21.81	4.30
NGC 4489	GON	E	0.198	1.690			
NGC 4494	BS	E	0.275	2.093	0.31	−19.17	3.18
NGC 4552	GON	E	0.324	2.417	0.45	−20.60	3.74
NGC 4636	DSP	E	0.311	2.281	0.93	−21.01	3.89
NGC 4649	GON	E	0.338	2.533	0.80	−21.45	4.15
NGC 4696	CDB	cD	0.277	2.348	1.79	−23.93	4.59
NGC 4697	GON	E	0.297	2.217	0.58	−20.08	3.55
NGC 4839	DSP	cD	0.315	2.413	1.13	−21.73	4.21
NGC 4874	FFI	cD	0.328	2.389			
NGC 5011	CDB	E	0.278	2.360	0.85	−21.89	3.94
NGC 5018	CDb	E	0.209	2.348	0.75	−21.95	3.85
NGC 5044	CDB	E	0.324	2.369	1.21	−21.88	4.21
NGC 5077	CDB	E	0.295	2.439	0.69	−20.86	3.94
NGC 5090	CDB	E	0.307	2.435	1.10	−22.42	4.22
NGC 5322	BS	E	0.276	2.350	0.56	−20.54	3.72
NGC 5638	GON	E	0.317	2.201	0.48	−19.67	3.45
NGC 5796	CDB	E	0.319	2.398	0.72	−21.66	3.90
NGC 5812	GON	E	0.324	2.310	0.61	−20.86	3.70
NGC 5813	GON	E	0.308	2.377	0.91	−21.29	4.00
NGC 5831	GON	E	0.289	2.220	0.64	−20.37	3.60
NGC 5846	CDB	E	0.321	2.444	1.13	−21.99	4.26
NGC 5903	CDB	E	0.270	2.371	0.91	−21.65	4.00
NGC 6127	GON	E					
NGC 6166	FFI	cD	0.340	2.513	1.62	−23.14	4.70
NGC 6702	GON	E	0.272	2.260	0.94	−21.14	3.86
NGC 6868	CDB	E	0.317	2.456	0.80	−21.24	4.04
NGC 7052	GON	E					
NGC 7097	CDB	E					
NGC 7192	CDa	cD	0.250	2.267	0.70	−20.39	3.70
NGC 7200	CDB	cD	0.282	2.290	0.60	−20.01	3.67
NGC 7454	GON	E	0.206	2.049	0.48	−19.49	3.24
NGC 7562	GON	E	0.291	2.386	0.81	−21.43	3.95
NGC 7619	GON	E	0.336	2.528	0.92	−21.63	4.22
NGC 7626	DSP	E	0.336	2.369	0.99	−21.64	4.05

TABLE 4—*Continued*

Galaxy	Ref.	Type	$(Mg_2)_0$ [mag]	$\log\sigma_0$ [km s^{-1}]	$\log R_e$ [kpc]	M_B [mag]	κ_1
(1)	(2)	(3)	(4)	(5)	(6)	(7)	(8)
NGC 7720	FFI	cD	0.339	2.484	1.20	−22.33	4.36
NGC 7768	FFI	E	0.322	2.384	1.11	−21.78	4.16
NGC 7785	GON	E	0.296	2.464	0.94	−21.83	4.15
IC 1459	CDB	E	0.321	2.489	0.73	−21.42	4.04
IC 3370	CDB	E	0.262	2.316	0.84	−21.29	3.87
IC 4889	CDB	E	0.244	2.246	0.60	−20.90	3.60
IC 4943	CDB	E	0.243	2.223	0.47	−19.30	3.48
Abell 496	FFI	E					
ESO 323-16	CDB	cD					

Col.(1).—Galaxy ID.

Col.(2).—Reference.

Col.(3).—Morphology.

Col.(4).—Central Mg_2 index.

Col.(5).—Central velocity dispersion.

Col.(6).—Effective radius in kpc

Col.(7).—Absolute magnitude in B-band.

Col.(8).—Mass tracer $\kappa_1 = (\log\sigma_0^2 + \log R_e)/\sqrt{2}$.

TABLE 5
GLOBAL SCALING RELATIONS

x	y	N	r	Regression Line
$[Fe/H]_0$	$\Delta Mg_2/\Delta\log r$	43	−0.21	
$\langle[Fe/H]\rangle$	$\Delta Mg_2/\Delta\log r$	46	0.22	
$\log\sigma_0$	$\Delta Mg_2/\Delta\log r$	43	0.17	
$\log R_e$	$\Delta Mg_2/\Delta\log r$	42	0.26	
κ_1	$\Delta Mg_2/\Delta\log r$	42	0.27	
M_B	$\Delta Mg_2/\Delta\log r$	42	0.33	
$\log\sigma_0$	$[Fe/H]_0$	43	0.45	$y = 0.76\,x - 1.73$
$\log\sigma_0$	$\langle[Fe/H]\rangle$	43	0.74	$y = 1.46\,x - 3.62$
$\log R_e$	$[Fe/H]_0$	42	0.22	
$\log R_e$	$\langle[Fe/H]\rangle$	42	0.33	
κ_1	$[Fe/H]_0$	42	0.37	$y = 0.20\,x - 0.71$
κ_1	$\langle[Fe/H]\rangle$	42	0.59	$y = 0.37\,x - 1.62$
M_B	$[Fe/H]_0$	42	0.19	
M_B	$\langle[Fe/H]\rangle$	42	0.37	
$\log\sigma_0$	$\langle[Mg/Fe]\rangle$	27	0.22	
$\log R_e$	$\langle[Mg/Fe]\rangle$	26	0.15	
κ_1	$\langle[Mg/Fe]\rangle$	26	0.00	
M_B	$\langle[Mg/Fe]\rangle$	26	0.21	

TABLE 6
FUNDAMENTAL PLANES

x	y	z	N	Regression Line
$\log\sigma_0$	$\log R_e$	SB_e	42	$x - 0.64\,y + 0.27\,z = 7.70$
$\log\sigma_0$	M_B	SB_e	42	$x - 0.09\,y + 0.12\,z = 3.17$
$(Mg_2)_0$	$\log R_e$	SB_e	42	$x - 0.26\,y + 0.13\,z = 2.80$
$(Mg_2)_0$	M_B	SB_e	42	$x - 0.04\,y + 0.09\,z = 1.41$
$\langle[Fe/H]\rangle$	$\log R_e$	SB_e	42	$x - 1.26\,y + 0.55\,z = 10.56$
$\langle[Fe/H]\rangle$	M_B	SB_e	42	$x - 0.16\,y + 0.28\,z = 2.41$